Quantum Dot-Based Thin-Film III–V Solar Cells

Quantum dot based thin film III-V solar cells

F. Cappelluti (1), A. Tukiainen (2), T. Aho (2), F. Elsehrawy(1), N. Gruginskie (3), M. van Eerden (3), G. Bissels (4), A. Tibaldi (1), G.J. Bauhuis (3), P. Mulder (3), A. Khalili (1), E. Vlieg (3), J.J. Schermer (3), M. Guina (2)

(1) Department of Electronics and Telecommunications, Politecnico di Torino, Cso Duca degli Abruzzi 24, 10129 Torino, Italy

(2) Optoelectronics Research Centre, Physics Unit, Faculty of Engineering and Natural Sciences, Tampere University, P.O. Box 692, 33101 Tampere, Finland

(3) Institute for Molecules and Materials, Radboud University, Heyendaalseweg 135, 6525 AJ Nijmegen, The Netherlands

(4) tf2 devices B.V., Heyendaalseweg 135, 6525 AJ Nijmegen, The Netherlands

Abstract In this work we report our recent results in the development of thin-film III-V solar cells fabricated by epitaxial lift-off (ELO) combining quantum-dots (QD) and light management structures. Possible paths to overcome two of the most relevant issues posed by quantum dot solar cells (QDSC), namely the degradation of open circuit voltage and the weak photon harvesting by QDs, are evaluated both theoretically and experimentally. High open circuit voltage QDSCs grown by molecular beam epitaxy are demonstrated, both in wafer-based and ELO thin-film configuration. This paves the way to the implementation in the genuine thin film structure of advanced photon management approaches to enhance the QD photocurrent and to further optimize the photovoltage. We show that the use of light trapping is essential to attain high efficiency QDSCs. Based on transport and rigorous electromagnetic simulations, we derive design guidelines towards light trapping enhanced thin-film QDSCs with efficiency higher than 28% under unconcentrated light, ambient temperature. If photon recycling can be fully exploited, 30% efficiency is deemed to be feasible. Towards this goal, results on the development and integration of optimized planar and micro-patterned mirrors, diffractive gratings and broadband antireflection coatings are presented.

Keywords: Solar cell - III-V semiconductors - Thin-film - Epitaxial lift-off - Quantum dot – Light trapping

1 Introduction

III-V semiconductors enable the highest efficiency solar cells demonstrated to date owing to their excellent optical and transport properties and a very mature technology. Single junction GaAs solar cells hit a record efficiency of 29.1% [1], very close to the Shockley-Queisser (SQ) limit [2] of 33.5 % under the terrestrial AM1.5G sun spectrum. The SQ limit sets the upper efficiency attainable by a single junction solar cell only based on the energy bandgap of the semiconductor material and the incident spectrum. The bandgap limits in fact at the same time the spectral sensitivity of the cell – i.e. the minimum energy of photons that can be converted into free charge carriers - and the maximum energy with which those carriers can be extracted from the cell, the excess energy being lost through carriers' thermalization processes. Fig. ***1*** shows the calculated SQ limit of single-gap solar cells for representative air-mass spectra in space (AM0), terrestrial (AM1.5G), and concentration photovoltaics (AM1.5D). One concept – the most successful to date - to improve the efficiency beyond the SQ limit, relies on stacking different semiconductor junctions which selectively absorb a fraction of the incoming sunlight, extending the harvested spectrum range and keeping the thermalization losses low [3]. The resulting multi-junction solar cell has a maximum theoretical efficiency of 67% under the AM1.5G spectrum [4]. The most common implementation relies on a two-terminal monolithic device wherein the subcells are series-connected through tunnel diodes. Thus, the current through the solar cell is limited by the subcell producing the lowest current and the key requirement is to divide the sun spectrum absorption among semiconductors with the right bandgap – to provide similar photocurrent - and that can be epitaxially grown together with high quality [5, 6]. Due to the richness of III-V materials in terms of bandgaps well matched to the sun spectrum and the relative ease to combine them, the conversion efficiency of multi-junction III-V solar cells has been increasing continuously for decades. Lattice matched, metamorphic, and wafer-bonded approaches have been developed [7]. The present record is over 46% [1, 8] and there are ample opportunities for further improvements.

While the present terrestrial photovoltaic industry is dominated by silicon cells, III-V's are the predominant technology for space and concentrator cells. For spacecraft applications, III-V solar cells have an unchallenged position owing to their high power-to-weight ratio and resistance against extreme conditions such as electron, proton and harsh UV radiation as well as cyclic temperature changes between plus and minus 100 ^{o}C. In spacecraft applications (i.e. under AM0), the industry's standard is provided by triple-junction III-V cells with a typical efficiency of 30%. Since they can handle large thermal loads and feature high open circuit voltages (V_{oc}), III-V solar cells are also highly suited for Concentrator PhotoVoltaic (CPV) systems. Such systems use cost-efficient concentrating optics to collect

the sunlight incident over a large area and focus this on a solar cell with a much smaller surface area to reduce the cost per unit output power. Typical concentration ratios are 500 to 1000 [9]. Commercially available multiple-junction III-V solar cells dedicated for CPV applications reach efficiencies up to 40% at these concentration ratios. With such high-efficiency cells CPV modules can have a lower Levelised Cost of Electricity (LCOE) than regular silicon solar modules in areas with high Direct Normal Irradiation (DNI) levels [10].

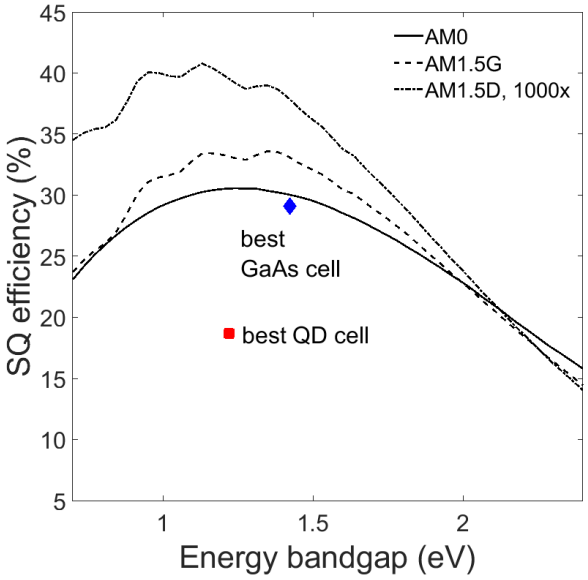

Fig. 1 Shockley-Queisser limiting efficiency curves for single-junction solar cells under AM0, AM1.5G and 1000 x AM1.5D spectra. For the sake of reference, also the record GaAs [1] and QD solar cell [11] are shown.

Worldwide research in III-V solar cells aims today at increasing their power/cost ratio by improving the output power and reducing the production costs. In fact, the high performance of III-V's comes at the price of a high cost, mainly dominated by the epitaxial growth and the wafer. In particular, multiple junction cells are the most complex to manufacture and inherently the most expensive, since they involve thick, complex epitaxial layers and, in some approaches, the use of multiple wafers. On the other hand, III-V semiconductors are generally optically thick, meaning that a few micrometres of active material are sufficient to harvest all the incident light. Therefore, a drastic cost reduction is possible if the epitaxial layers can be separated from their wafer, which only serves during the growth process, and the wafer can be re-used several times. Thin film III-V technologies based on epitaxial lift-off (ELO) [12–14] are among the most promising approaches to attain III-V cells with high efficiency/cost ratio. Besides the remarkable reduction of cost, the thin-film architecture enables the integration of

mirrors to implement photon trapping and recycling mechanisms that are essential to reach the highest efficiency [15–17]. As a matter of fact, the world-record single-junction cell is an ELO thin-film GaAs cell [14, 1]. Besides the development of a useful wafer separation and reuse technology, the reduction of chemical vapor deposition costs - by increasing the cell deposition rate and reducing the cell thickness - and the development of alternative cell deposition technologies are key research areas towards the development of low cost III-V photovoltaics [18]. In this regard, light trapping plays again an important role because enabling electrically thin layer (with respect to the diffusion length) may relax the requirements in terms of crystal quality. The improvement of power output of multiple junction cells encompasses a) optimization of the efficiency of each individual subcell; b) development of alternative subcells with a better response to the dominant illumination condition; c) adding more junctions (subcells) to the device. With respect to b), a point of attention for series-connected multi-junction cells is related to the large spectral sensitivity to changes of the solar spectrum that impacts their annual energy production capacity [6, 19–21]. Therefore, alternative architectures such as multi-terminal devices with independently connected subcells are receiving renewed attention [22, 23].

Nanostructured absorbers such as quantum well (QW) and quantum dot (QD) materials offer a complementary path to further developing III-V photovoltaics. With respect to the research directions a)-c), bandgap engineering in QWs [24] and QDs [25] is an attractive solution for the spectral tuning and optimization of multijunction cells [26, 27]. Moreover, single junction nanostructured solar cells can match the optimum bandgap at high concentration – around 1.2 eV at 1000 sun, see Fig. 1– and achieve 40% efficiency with a simpler – and possibly less expensive - technology and more stable performance under spectral fluctuations [27, 28]. In space applications, QDs may bring additional benefits such as enhanced radiation tolerance [26]. Finally, owing to their tunable optoelectronic characteristics, quantum-confined materials are among the most promising material platforms for introducing next generation photovoltaic concepts. In particular, QD solar cells (QDSCs) have been extensively investigated both theoretically and experimentally for the implementation of the intermediate band solar cell (IBSC) [29, 30].

As well known, QDs introduce 3D potential wells within the host semiconductor, confining carriers in energy states within the host semiconductor forbidden energy band. Under sun illumination, charge carriers are photogenerated in the extended and bound states through interband and intraband optical absorption. Depending on the effectiveness of thermalization of photogenerated carriers from the extended to the bound energy states, two different situations arise in the photovoltaic process:

- If intraband carrier thermalization is slow with respect to radiative recombination (and conversely, thermal escape is slow with respect to photon assisted escape), a non-equilibrium condition exists between the continuum and the confined states sustained by a two-step photon absorption process [29]. The result is an enhanced short circuit current that does more than compensate for the small reduction of V_{oc} due to the reduced bandgap of

the nanostructured material. The SQ limit is therefore overcome breaking the trade-off between spectral harvesting and thermalization loss of conventional single junction cells.

- If intraband carrier thermalization is instead faster than radiative recombination, the continuum and confined states are in thermal equilibrium and the solar cell operates somewhat similarly to a single-junction cell of bandgap lower than the host semiconductor. In this case the limiting efficiency is arguably still provided by the SQ limit. We refer to this second class of devices as thermally-limited QDSC.

From the experimental standpoint, even though the ground principles of the IB concept have been proven [30, 31], QDSCs usually fall in the thermally-limited case. A clear enhancement of the infrared spectral response is observed in these devices, but the maximum demonstrated efficiency (18.7% at 1 sun for a InAs/GaAs QDSC) [11] lags well behind that of state-of-art GaAs single-junction cells, not to mention the gap with respect to the efficiency predicted by the IB theory (≈ 36% for the InAs/GaAs material system at 1 sun). The large discrepancy between demonstrated and theoretical efficiency is often ascribed to the fact that reported devices work in the thermally-limited regime. However, under such conditions a conservative benchmark value for the attainable efficiency is given by that of a single-junction cell with bandgap comparable to the optical transition energy of the QD ground state. Assuming a band gap of 1 eV (representative of the InAs/GaAs QD system) the SQ limit efficiency is above 30% under 1 sun, a value remarkably higher than the demonstrated one.

There are two main problems to overcome for achieving high efficiency QDSCs, regardless if they fall in the IB or thermally limited class. First, the small optical absorption cross-section of QDs and their reduced volume fraction within the absorber material make the extended absorptivity provided by the QDs quite low, whereas the SQ theory assumes complete absorptivity for above-gap photons. The requirements are even more demanding to approach the IB operating regime, since very high – and comparable – interband and intraband photon absorption [31] would be needed. Based on detailed balance calculations, InAs/GaAs IBSCs require a QD density larger than 5×10^{13} cm^{-2} [32], but present QDSCs usually have a few tens of layers and in-plane density about $\times$ 5 10^{10} cm^{-2}. The second fundamental issue is related to the reduction of V_{oc}. While this is in part an *intrinsic* effect, because the large electrical confinement of electrons and holes leads to enhanced radiative recombination at the QD sites (or equivalently the cell effective bandgap is narrowed by the QDs), reported devices are often plagued by further *extrinsic* loss due to defect mediated recombination. Such defects are induced by the crystal strain inherent to the QD growth. Strain compensation techniques are therefore demanded during the epitaxial growth and have led to the demonstration of high V_{oc} QDSCs with low extrinsic loss [33].

To enhance the QD photogeneration, significant research efforts are devoted to grow high quality crystals with increased QD sheet density [34–37] and number of QD layers [38, 39]. However, the intrinsic V_{oc} penalty also increases

with the number and density of QD layers. Theoretical calculations show that such efforts will give frustrating results in terms of cell efficiency improvement, unless they are combined with clever ways to further increase the QD absorptivity [40, 41]. This calls for the development of light trapping approaches that can be implemented within a thin-film solar cell architecture [28, 42, 43]. ELO thin-film InAs/GaAs QD cells with planar rear mirror were first reported in [44, 45]. In [40] we have demonstrated a two-fold increase of QD photocurrent in an InAs/GaAs QDSC fabricated by ELO, however the cells – either QD and bulk ones - suffered of a high V_{oc} degradation due to a non-sufficient quality of the epilayers.

In this chapter, we report our most recent results in the development of high efficiency thin-film III-V QD solar cells, with high V_{oc} and enhanced QD photon harvesting. Sec. 2 reviews the ELO method and discusses the optimum junction configuration for thin-film III-V cells approaching the radiative limit operation. In Sec. 3 we study extrinsic and intrinsic V_{oc} loss with the help of device-level physics-based simulations and report our latest achievements in the molecular beam epitaxy growth of high voltage QDSCs. The implication of the intrisic V_{oc} penalty and the demand for light trapping approaches are discussed in Sec. 4, where we summarize our work on the development of photon management approaches in thin-film III-V QDSCs. After the demonstration of high V_{oc} ELO QD cells with planar reflectors, Sec. 4 discusses the design and fabrication of back surface reflectors and nanostructured antireflection coating for effective light trapping. Finally, an approach for enhanced photon recycling in thin-film cells by a highly reflective patterned rear contact/mirror is presented.

2 Epitaxial Lift-Off for genuine thin-film III-V devices

Most III-V materials are direct band-gap semiconductors with high absorption coefficients. Therefore, the active structure in a III-V solar cell only needs to be several microns thick to absorb all the light that the cell can convert into electricity. Nevertheless, III-V solar cells are referred to as a wafer-based technology because in order to produce high quality single crystal III-V structures, state of the art low defect single crystal InP, GaAs or Ge wafers are required as a production platform. After deposition of the cell structure, the wafer is of no further use. However, in the present fabrication techniques the thin active structure is processed together with its passive substrate to become a wafer-based solar cell (see Fig. 2 left).

Compared to the manufacturing methods used nowadays, the amount of precious semiconductor material used to generate a certain output power can be reduced by two orders of magnitude by the utilisation of a thin-film separation technology that allows to reuse the native wafer (which is about 100 times thicker than the active cell structure on top of it) as a production platform. The epitaxial lift-off (ELO) method offers the opportunity to separate thin-film III-V structures

from their original wafer substrate [46–49] and transfer them to a low cost foreign carrier like glass or plastic for stability during further processing and application. In order to apply the ELO method, a typically 10 nm thick $Al_xGa_{1-x}As$ ($x > 0.6$) release layer has to be deposited before the actual III-V device structure (see Fig. 2 right). This sacrificial layer allows for the separation of the device structure from its substrate by selective wet etching using an aqueous hydrofluoric (HF) solution. Owing to the large selectivity ($>10^6$) of the HF solution for etching of AlGaAs over GaAs [50, 51], the original substrate is hardly affected. ELO reaction residues, mainly elemental arsenic, form As_2O_3 crystallites over time [52]. However, with an appropriate surface re-preparation strategy (e.g. a polishing etch or removable protection layer) the substrate can be reused [13, 53–56].

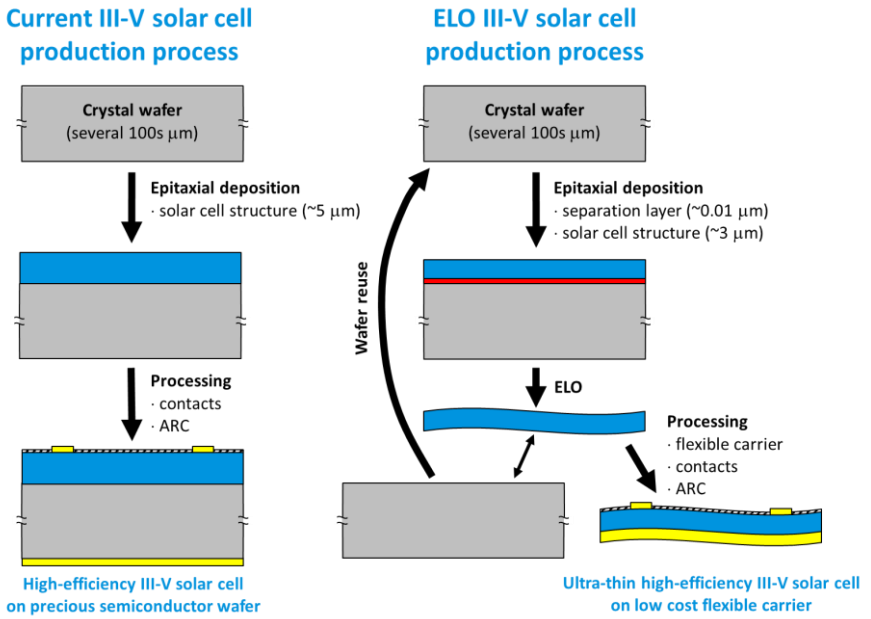

Fig. 2 Schematic representation (not to scale) of the current production process for wafer-based III-V cells (left) and thin-film cells via the epitaxial lift-off technology which facilitates reuse of the wafers (right).

The first attempts to separate III-V devices from their substrates using the extreme selectivity of an aqueous HF solution for AlGaAs over GaAs were described as early as 1978 [46]. A wax layer was applied to support the circa 30 µm thick fragile films during the process which at that time was referred to as 'Peeled Film Technology'. Almost a decade later, it was noted that if the film structures have a thickness in the range of a few micrometres, the tension induced by the wax support layer causes the III-V films to curl up as they become undercut [47]. This was concluded to be beneficial for removal of the etch products during the process. As a result, the lateral etch rate of the AlGaAs release layer with a typical

thickness in the 10-100 nm range increased to about 0.3 mm/h [57]. After etching of the sacrificial AlGaAs layer the surface morphology of the thin-film device structures typically shows an increased surface roughness and the presence of reaction residues [52,71]. This has no consequences for the performance of the final devices as the epilayer structure can be designed in such a way that the outer layer affected by the substrate removal process is non-critical (e.g. a contact layer) or is etched away completely during subsequent device processing.

Using this process, now referred to as 'Epitaxial Lift-Off technique', many III-V devices such as solar cells [58–60], photodiodes [61, 62], LEDs [63, 64] , LASERs [65, 66], HEMTs [67], FETs [68] and THz-antennas [69] transferred to silicon, silicon-oxide, sapphire and glass plates were demonstrated. However, because the etch rate still was fairly low, the demonstrated devices were generally limited from several millimetres up to a square centimetre size.

2.1 Rapid release of full wafer size thin-film structures for photovoltaic applications

At Radboud University the parameters influencing the ELO etch process were systematically investigated [48, 70–72] and a model to describe the etch process was developed [73, 74]. By making some essential modifications like mounting a temporarily flexible carrier/handle on top of the III-V epi-structure and applying a controlled force to bend the carrier with the epi-structure away to allow the etchant to reach the etch front, the lateral etch rate increased more than 100 times to well over 30 mm/hr [74–76]. At the same time the flexible foil and increased etch rate offered the possibility to increase the lateral size of the released III-V structures from typically a square centimetre to full wafers ranging from 2-in up to 6-in diameter [12, 13, 49, 77, 78]. Besides structures from GaAs wafers, ELO has also been successfully demonstrated for Ge and InP wafers, as well as multiple-times reused wafers. The method has successfully been demonstrated for a whole range of solar cell structures, such as single- and multi-junction, inverted and upright, lattice matched and metamorphic structures as well as structures containing quantum dots. Both III-V epi-structures produced by Metal Organic Vapour Phase Epitaxy (MOVPE) and by Molecular Beam Epitaxy (MBE) can be processed by ELO. Automated ELO production equipment has also been developed, as shown in Fig. 3. Examples of thin-films released from 2-in and 4-in diameter wafers are shown in Fig. 4.

Fig. 3 Automated ELO processing equipment developed at tf2-devices.

Fig. 4 Wafer-sized thin-film structures retrieved from 2-in (upper) and 4-in (lower) diameter GaAs substrates by epitaxial lift-off using a flexible carrier/handle.

After ELO the III-V solar cell structure can, by flipping from one temporary carrier to another, be processed on both sides. Together with the final carrier to be applied, this allows for new device structures which can be optimized for different purposes. The carrier can be a lightweight material for space applications [60, 79], a flexible carrier to cover bended surfaces [80, 81], a heat conducting material for concentrator applications or any type of low bandgap cell to form a mechanically stacked multi-junction solar cell [49, *82*, 83]. In case of a transparent carrier the thin-film cell can be processed with a grid contact pattern on both sides. In this way semi-transparent or bifacial III-V solar cells are obtained [*84*, 85]. Alternatively, an arbitrary carrier can be applied to support a thin-film cell with a full back contact. If applied correctly this back contact might at the same time act as a mirror which reflects any photons that reach the rear side of the cell back into the cell structure [85, 86]. Fig. **5** shows some examples of solar cells produced from thin-film III-V structures that were released from 4-in wafers.

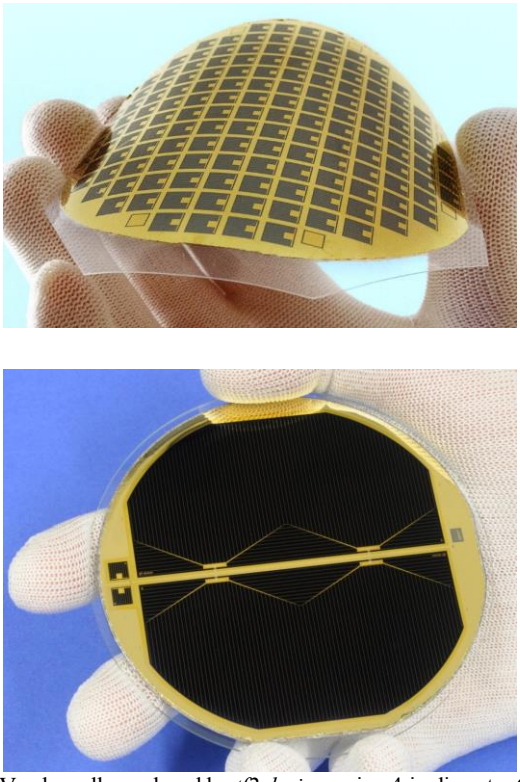

Fig. 5 Thin-film III-V solar cells produced by *tf2 devices* using 4-in diameter GaAs substrates as a production platform followed by ELO and thin film cell processing. Top: array of 5x5 mm^2 ELO solar cells on a flexible carrier, bottom: two 30 cm^2 ELO solar cells on a rigid carrier.

The deposition of III-V epi-structures for ELO thin-film solar cells typically is performed by MOVPE [13, 87], but structures produced by MBE [40, 45] work equally well. It is however essential to utilise epi-structures of sufficient quality. Owing to photon recycling, i.e. the excitation of electrons resulting from reabsorption of photons generated by radiative recombination of electrons and holes [88–91], for state of the art epi-structures, thin-film ELO solar cells typically outperform their substrate based equivalent cells [92]. This is clearly demonstrated by the present power conversion efficiency world records for single junction GaAs solar cells being 27.8% for a substrate-based and 29.1% for the thin-film ELO cell [1]. On the other hand, epi-structures of lesser quality might suffer from the ELO etch process, resulting in a reduced cell performance of the ELO thin-film cells compared to their substrate based equivalent. In case of inferior epi-structures, the difference in cell performance will be huge, and directly apparent from the Electro-Luminescence (EL) analysis of the devices [40]. For regular state of the art epi-structure quality the EL signals of thin-film and substrate based cells typically show no defects whatsoever and differences in cell performance can only be judged from the I-V and EQE characteristics.

2.2 Shallow- and deep-junction configurations

III-V solar cells are typically produced in a n-on-p shallow-junction (SJ) geometry, i.e. with a thin highly doped n-type emitter and a thick p-type basis. The shallow junction geometry ensures that most of the light is absorbed close to the p-n junction, thus minimizing the constraints on the free carrier lifetimes. However, with the high quality of the epi-layers that are currently obtained by MOVPE and MBE, carrier lifetimes are sufficiently high to allow for n-on-p cells in a deep-junction (DJ) configuration [93–95]. In a comparative study substrate-based DJ GaAs and InGaP cells demonstrated to perform better than their SJ counterparts [96]. This is because at the maximum power point the DJ cells operate mainly in the radiative recombination regime (ideality factor n = 1.22), while in the SJ cells non-radiative recombination is dominant (n = 1.86). As shown in Fig. 6, the steeper slope of the IV curve of the DJ cell boosts the fill-factor by about 5%, which is thereby the most improved cell parameter. In order to minimize collection losses in the upper part of the solar cell, the optimal thickness (h) of the emitter plus base of the GaAs DJ cell is only 2.5 μm compared to 3.2 μm for the SJ cell. Nevertheless, the associated lower cell current is more than compensated by the higher fill-factor and open circuit voltage and as a result the efficiency of the cell is raised from 25.2% for the SJ GaAs cell to 26.5% for the DJ cell. In the thinner InGaP cell the absence of current loss resulted in an even larger efficiency benefit for the DJ geometry (18.2% as compared to 16.6%) [96].

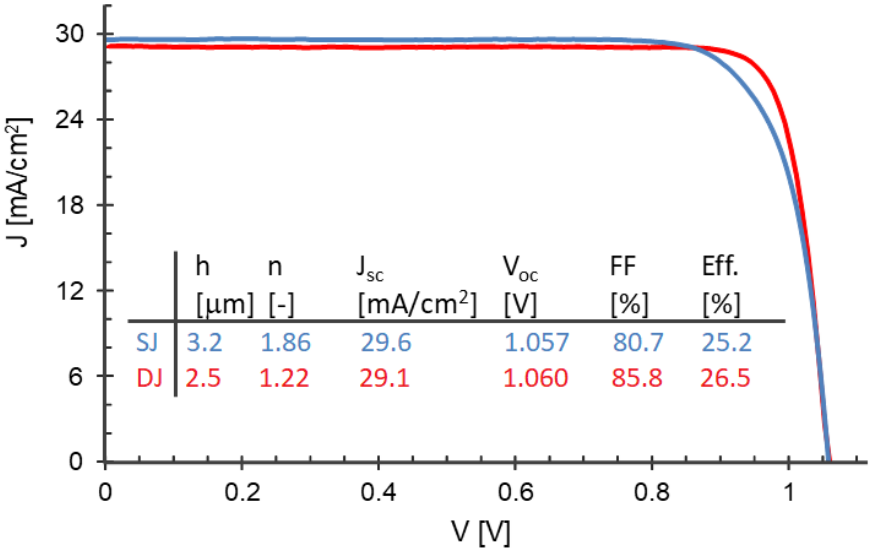

Fig. 6 J-V characteristics of 1 cm^2 substrate-based shallow-junction and deep-junction GaAs cells. The cells were processed with optimal anti-reflective coatings and a front grid that covers only 1.5% of the cells surface.

3 High V_{oc} InAs/GaAs QD solar cells by MBE growth

InAs QDs embedded in GaAs exhibit a small bandgap and induce a large electrical confinement for electrons and holes. The strong carrier confinement leads to enhanced carrier recombination at the QD sites, which results in an intrinsic reduction of the V_{oc}. Also, every grown InAs QD layer results in excessive compressive strain which eventually leads to formation of lattice defects manifesting as dislocation lines and a further extrinsic reduction of the V_{oc}. Recently, it has been demonstrated that by using metal-organic chemical vapor deposition (MOCVD) it is possible to fabricate InAs/GaAs QD solar cells with V_{oc} close to 1 V and only a marginal V_{oc} reduction compared to GaAs reference solar cells [33, 97]. On the other hand, using molecular beam epitaxy (MBE), another viable and mass-production capable epitaxy method, such high Voc values for InAs/GaAs QD solar cells were not published for long time. The published Voc values for MBE-grown InAs/GaAs QD solar cells have typically been about 0.2 V lower than the Voc values of high quality GaAs reference solar cells [11, 40, 98, 99]. This has been partially due to larger QDs used in the structures or due to increased recombination at the QD regions. However, when comparing the works done using MOCVD or MBE it is important to understand that for both techniques the Voc values degrade for larger QDs in very similar manner [11]. Recently, the authors have demonstrated that InAs/GaAs QD solar cells with high V_{oc}, approaching 0.95 V, can be fabricated also by MBE [100].

In this section we present an assessment of the typical intrinsic and extrinsic V_{oc} reduction mechanisms in QDSCs based on the study of experimental devices by quantum-corrected transport simulations. Then, we review the fabrication of MBE-grown high-V_{oc} InAs QD solar cells and discuss the characteristics of deep junction and shallow junction structures [100].

3.1 Causes for V_{oc} reduction in QDSCs

3.1.1 QD-corrected transport model

Models of QDSCs have been traditionally developed based on the hypotheses of IB operation, with detailed balance [101–103] and in some cases with drift-diffusion [104–106] approaches. Recently, a detailed balance model of thermally limited QDSCs has been reported in [107], suggesting a substantial equivalence between these devices and bulk cells. When it comes to understand the detailed physics of real devices and provide useful guidelines to their development, transport models become essential tools. However, the accurate device level modelling of QDSCs is a difficult task since it requires to manage details both at the nano/mesoscopic and at the microscopic scales. Novel quantum-kinetic approaches [108] are very well suited for nanostructure modelling but the available compu-

tational resources prevent to date their application to device-level simulations. In [109] an effective medium approach was developed to study the performance of QD multi-junction cells, where the QD recombination and related V_{oc} loss is somehow modelled by describing the QDs as equivalent trap states. Recently, Polytechnic of Turin has developed a quantum-corrected drift-diffusion simulator that, including the peculiar physics of the QD material, leads to an accurate description of the interband and intersubband charge transfer processes involved in QDSCs operation. The initial works [110, 111] demonstrated the impact of such processes on intrinsic and extrinsic V_{oc} reduction and a number of follow-up papers have applied the model to the analysis of real solar cells and to the design of high efficiency QDSCs [40, 43, 112, 113].

To focus the ideas one can consider the solar cell structure and the associated band diagram in Fig. 7b. A DJ n-p solar cell embeds a stack of 20 QD layers with undoped interdot layers. The QD stack is placed next to the junction to ensure optimal carrier collection at short circuit. As sketched in Fig. 7c, the three-dimensional confinement of carriers in the QDs introduces subband gap energy states modeled by three discrete energy levels in the conduction and valence band: ground state (GS), excited state (ES), and wetting layer (WL). At each QD layer, possible interband and intraband charge transfer mechanisms include intersubband relaxation and excitation, photogeneration, and radiative recombination. Within the present work we assume that charge transfer between subband energy states occurs only through thermal cascaded capture and relaxation, because at room temperature, for the InAs/GaAs material system, optical intersubband processes are negligible with respect to the thermally activated ones [114]. On the other hand, the model can be extended to deal with intersubband optical transitions in material systems with relatively higher energy band separations (or for lower operating temperature) where thermal transitions are reduced [115, 116].

The QDSC operation can be described as follows: electron and holes are photogenerated in the barrier and QD states by above and below energy gap photons, respectively. Bulk carriers move by drift-diffusion and when they fall within the QD interaction range (a few nm), they can either be emitted through the QD

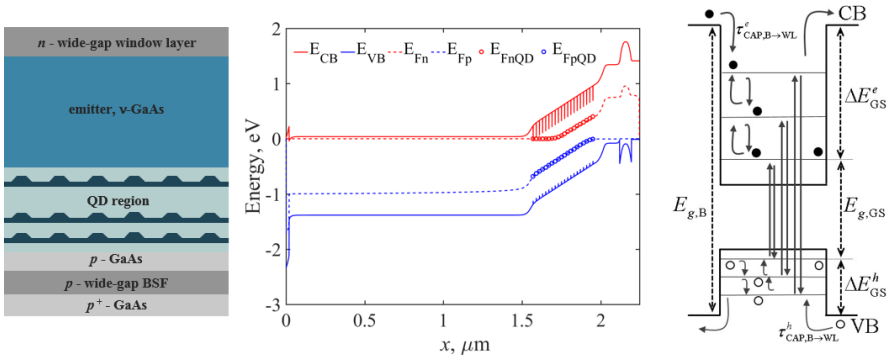

Fig. 7 Sketch of the studied GaAs n-p solar cell with embedded QD layers and the corresponding energy band diagram at short-circuit condition under AM1.5G illumination. On the right, QD energy states and interband and intersubband transitions considered in the model.

layer or captured in QD states. Capture and escape mechanisms connecting the bulk and the bound states are mediated by the WL states. To account for this, 3D carriers continuity equations and Poisson equation for the electrostatic potential are corrected with terms accounting for capture/escape processes and QD occupation:

$$\frac{\partial n}{\partial t} = \frac{1}{q}\frac{\partial J_n}{\partial x} - U_n^{\mathrm{B}} + G_{\mathrm{ph}}^{\mathrm{B}} - \sum_i \left(R_{n,\mathrm{cap}}^{\mathrm{B}\to\mathrm{WL},i} - R_{n,\mathrm{esc}}^{\mathrm{WL},i\to\mathrm{B}}\right)\delta\left(x - x_i\right) \tag{1}$$

$$\frac{\partial^2 \phi}{\partial x^2} = -\frac{q}{\epsilon}\left(p - n + N + \sum_{i,k}\left(p_{k,i} - n_{k,i}\right)\delta\left(x - x_i\right)\right) \tag{2}$$

where i identifies the QD layer, n the electron density, J_n the electron current density, $G^{\mathrm{B}}_{\mathrm{ph}}$ the photogeneration rate, and U_n^{B} the net recombination rate due to radiative and non radiative recombination, modeled according to Shockley-Read-Hall (SRH) theory. An equation analogous to (1) holds for holes.

The charge transfer between bulk and the QDs are treated locally near the i-th QD layer by carrier capture ($R_{n,\mathrm{cap}}^{\mathrm{B}\to\mathrm{WL},i}$) and escape ($R_{n,\mathrm{esc}}^{\mathrm{WL,i}\to\mathrm{B}}$) rates. The modified Poisson equation accounts for the local charge contribution of the QD states ($p_{k,i}$ and $n_{k,i}$ with k identifying the GS, ES and WL state).
Intersubband charge transfer is governed by rate equations for each QD state describing the subband population in the i-th QD layer as follows:

$$\frac{\partial n_{\mathrm{WL},i}}{\partial t} = R_{n,\mathrm{cap}}^{\mathrm{B}\to\mathrm{WL},i} - R_{n,\mathrm{esc}}^{\mathrm{WL},i\to\mathrm{B}} - R_{n,\mathrm{cap}}^{\mathrm{WL},i\to\mathrm{ES},i} + R_{n,\mathrm{esc}}^{\mathrm{ES},i\to\mathrm{WL},i} - U^{\mathrm{WL},i} + G$$

$$\frac{\partial n_{\mathrm{ES},i}}{\partial t} = R_{n,\mathrm{cap}}^{\mathrm{WL},i\to\mathrm{ES},i} - R_{n,\mathrm{esc}}^{\mathrm{ES},i\to\mathrm{WL},i} - R_{n,\mathrm{cap}}^{\mathrm{ES},i\to\mathrm{GS},i} + R_{n,\mathrm{esc}}^{\mathrm{GS},i\to\mathrm{ES},i} - U^{\mathrm{ES},i} + G$$

$$\frac{\partial n_{\mathrm{GS},i}}{\partial t} = R_{n,\mathrm{cap}}^{\mathrm{ES},i\to\mathrm{GS},i} - R_{n,\mathrm{esc}}^{\mathrm{GS},i\to\mathrm{ES},i} - U^{\mathrm{GS},i} + G$$

where $n_{\mathrm{GS},i}$, $n_{\mathrm{ES},i}$ and $n_{\mathrm{WL},i}$ are the electron sheet densities in the GS, ES and WL. $U^{k,i}$ and $G^{k,i}_{\mathrm{ph}}$ are net band to band recombination and photogeneration rates in the k-th state. Capture and escape processes depend on the occupation probability in each state and characteristic scattering times. In particular, the detailed balance at thermal equilibrium implies that escape and capture times are related by

$$\tau_{n,\mathrm{esc}}^{k-1,i} = \frac{N_{k-1}}{N_k}\tau_{n,\mathrm{cap}}^{k-1,i}\exp\left(\frac{E_k - E_{k-1}}{k_{\mathrm{B}}T}\right)$$

N_k being the effective density of states of state E_k.

QD electronic structure, optical properties, and scattering rates for the charge transfer mechanisms can be derived from quantum-mechanical models or from experimental data. In the following examples carrier capture and relaxation times between the QD states range on a scale of 100 fs for holes and 1 ps for electrons, while 1 ns radiative lifetime is used for all the QD levels [110].

Finally, the electrical model is coupled to a suitable optical model for the calculation of the spatially resolved photogeneration rates [40, 112].

3.1.2 Intrinsic and extrinsic V_{oc} loss

To clarify the issue of V_{oc} degradation in QDSCs it is helpful to analyze a real life example with the help of the quantum-corrected model described in Sec. 3.1.1. Fig. ***8*** reports the EQE and J-V characteristics of two InAs/GaAs QDSCs with 20 and 50 QD layers, respectively, and a reference GaAs cell [40]. The cells have an n-p+ structure, with the junction located close to the rear side contact and emitter thickness of 2 µm. In the QDSC samples a portion of the emitter is replaced by an intrinsic stack of QD layers with interdot spacing of 20 nm and areal density of 8 x 10^{10} cm^{-2}. QDs were grown by a Sb mediated technique to achieve high density without using any strain balancing compensation [36].

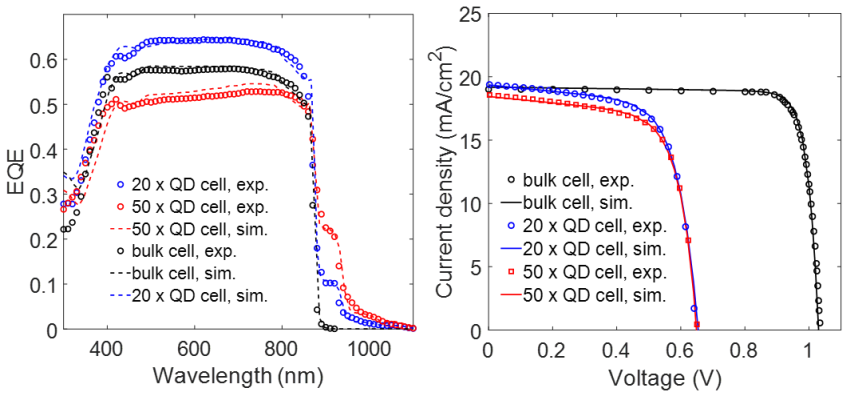

Fig. 8 Measured and simulated EQE spectra (left) and J-V characteristics (right) of a GaAs regular cell, a 20× QD cell, and a 50× QD cell. Reprinted from Sol. Energy Mater. Sol. Cells, 181, F. Cappelluti et al., Light-trapping enhanced thin-film III-V quantum dot solar cells fabricated by epitaxial lift-off, pp.83-92, Copyright (2018), with permission from Elsevier.

From the analysis of the PhotoLuminescence (PL) spectra of precursor samples with one QD layer and of the sub-bandgap EQE, the GS, ES and WL optical bandgaps result as 1.17 eV, 1.25 and 1.37 eV, 80% of which is attributed to the electron confinement energy in the conduction band [117]. In the QD layers, the optical absorption associated to each interband transition is modeled by a Gaussian function with absorption peaks on the order of 10^3 cm^{-1} for GS and ES states, and 10^4 cm^{-1} for WL state. The full list of QD and bulk material parameters used in this study is summarized in [40].

The experimental results in Fig. 8 point out a clear reduction of the collection efficiency of the 50 x QD cell with respect to the 20 x QD one and the reference cell, well visible from the EQE spectra, and a large and almost identical V_{oc} penalty in the QDSCs with respect to the reference cell. From the simulation study it turns out that the main factors affecting the cell operation are the minority carrier lifetime in the emitter and the non radiative recombination in the intrinsic barrier layers of the QD stack. In particular, SRH recombination in the emitter significantly impairs the short circuit current (which in such rear side junction cell sustains most of the short circuit current), while it has a lower impact on the V_{oc}. Viceversa, a decrease of the SRH lifetime in the intrinsic interdot layers of the QD stack has a limited impact on carrier collection, but affects strongly the recombination current and thus is responsible for the observed low V_{oc} in the QDSCs. Fig. ***9*** shows the predicted behaviour of the QDSCs V_{oc} as a function of the SRH carrier lifetime in the GaAs barrier layers. A range of SRH lifetimes in the low doped portion of the emitter is considered, which provides a reasonable fit to the EQE spectra of the 50x QDSC (about 3 ns) and of the 20x QDSC (15 ns – 200 ns depending on the specific sample). It is worth noticing that these cells were grown

without any strain management. The reduction of the SRH lifetime in the emitter of the 50x cell with respect to the 20x one suggests a higher defect density correlated to the larger number of QD layers and the higher strain accumulation during the epitaxial growth. As long as the SRH lifetime in the QD stack is significantly larger than the QD radiative lifetime (1 ns), the V_{oc} remains high with calculated limiting values (for negligible SRH recombination) on the order of 900 mV – denoting an intrinsic penalty of about 150 mV with respect to the reference cell due to the radiative recombination through the QD states, Therefore, in the samples under study the observed large reduction of V_{oc} can be attributed to crystal quality degradation, with an estimated SRH lifetime in the QD stack on the order of 100 ps.

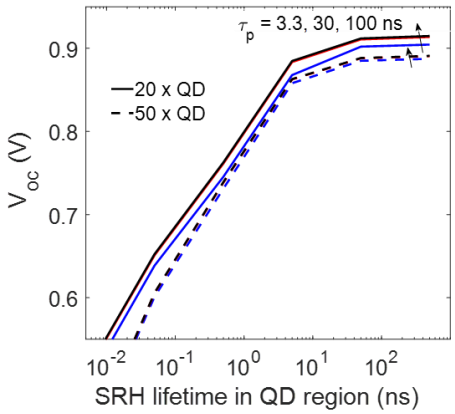

Fig. 9 Behavior of V_{oc} for the 20× (solid lines) and 50× (dashed lines) QD cells as a function of the SRH lifetime in the interdot layers of the QD stack, and for different values of SRH hole lifetime in the doped portion of the emitter (τ_p). Reprinted from Sol. Energy Mater. Sol. Cells, 181, F. Cappelluti et al., Light-trapping enhanced thin-film III-V quantum dot solar cells fabricated by epitaxial lift-off, pp.83-92, Copyright (2018), with permission from Elsevier.

Concerning the intrinsic V_{oc} loss, Fig. 10 shows some calculated trend in terms of V_{oc} scaling with the number of QD layers (N_S), QD areal density (N_{QD}), and GS emission energy under the hypothesis of negligible non radiative recombination. As shown in Fig. 10 (left), the intrinsic V_{oc} scales linearly with the natural logarithm of the number of layers, with a slope of 26 mV. At open circuit, $V_{oc} = V_T \ln(J_{sc}/J_0)$, where J_0 is the reverse saturation current, J_{sc} the short-circuit current density, and $V_T = 26$ mV. Since J_{sc} is weakly affected by the number of QD layers, the linear scaling of V_{oc} with $\ln(N_S)$ denotes an almost linear increase of the radiative recombination with N_S. Similar considerations can be drawn for the V_{oc} scaling with the areal density N_{QD}. In Fig. 10 (right) the intrinsic V_{oc} is analysed for different GS emission energies. This demonstrates that the linear scaling with $-V_T \ln(N_S)$ holds regardless of the confinement energy of carriers, since V_{oc} increases

almost linearly with the GS bandgap. The reason is that QDs act as trap centers whose activation energy increases as the confinement energy decreases, i.e. as thermal escape becomes more effective. From the experimental standpoint, a linear trend of V_{oc} with the E_{GS} was verified in [11] and more recently in [100] for high quality QDSCs, with a promising GS bandgap-voltage offset ($W_{oc}=E_{GS}/q - V_{oc}$) as low as 0.3 V, comparable to the highest efficiency thin-film GaAs cells. For reference, the theoretical offset is 0.36 V for radiative-limited GaAs cells [118], while 0.4 V is the value of state-of-art wafer-based GaAs cells. However, the results in Fig. 10 show that the bandgap-offset in nanostructured absorbers significantly depends on the QD volume density, and changes from about 0.15 V for the case with lowest volume fraction (low density and low number of layers) to about 0.35 V for the case with highest volume fraction. In fact, as the QD volume occupation increases, the onset of significant QD absorption becomes closer to the GS bandgap and W_{oc} approaches the typical value found for III-V bulk solar cells with radiative recombination only. On the other hand, in samples with low volume occupation, the offset is significantly lower. In this case, as noted in [119], the W_{oc} is no more a useful figure of merit to predict the efficiency potential of the cell, because the hypothesis of almost full absorptivity above the bandgap energy does not hold anymore. Nevertheless, as done in Sec. 3.2.5, the calculated intrinsic W_{oc} still provides a useful benchmark to quantify in real devices the extrinsic V_{oc} loss due to non radiative recombination.

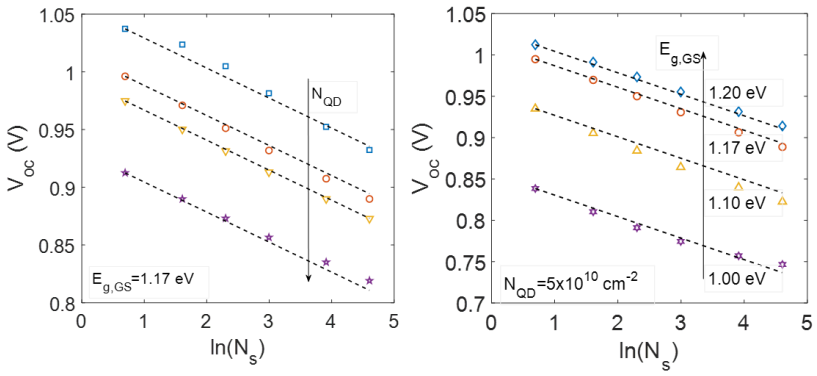

Fig. 10 Left: Scaling of V_{oc} with the number of QD layers (N_S) and QD areal density (N_{QD}= 1×10^{10}, 5×10^{10}, 1×10^{11}, 1×10^{12} cm^{-2}) for GS bandgap of 1.17 eV. Right: Scaling of V_{oc} with the number of QD layers and the GS bandgap for fixed areal density $N_{QD}=5\times10^{10}$ cm^{-2}. Symbols are results of simulations, dashed lines are linear fit according to $V_{oc} = V_T \ln(J_{sc}/J_0) \propto -V_T \ln(N_S)$, with V_T=26 mV.

3.2 Molecular-beam-epitaxy-grown InAs/GaAs quantum dot solar cells with high open circuit voltage

3.2.1 Experimental details

The samples were grown on p-GaAs(100) substrates using either a V90 or a V80H MBE system equipped with effusion cells for group-III elements and dopants, and valved cracker sources for group-V elements. Silicon and beryllium were used as n-type and p-type dopants, respectively. The nominal layer structures for DJ and SJ architectures are shown in Fig. 11. Growth temperature for the p-GaAs, n-GaAs, and p-AlGaAs BSF layers was kept at about 580°C. The lattice-matched n-AlInP window layer was grown at 490°C and the InAs QDs were grown at 465–475°C. The nominal amount of deposited InAs, determined by simple ion gauge flux measurements, was varied between 1.6 monoatomic layer (ML) and 2.2 ML to adjust the QD size. The QD density was targeted to be over 5×10^{10} cm^{-2}. A set of samples was grown without any strain management and in some samples thin, 2-monolayer-thick, GaAsP layers were inserted within the undoped GaAs barrier layers between the QD sheets for managing the accumulating compressive strain [33]. The number of QD sheets was varied between 0 and 20 to study the effects of increasing the active InAs QD volume on the photogeneration and structural behavior of the solar cells.

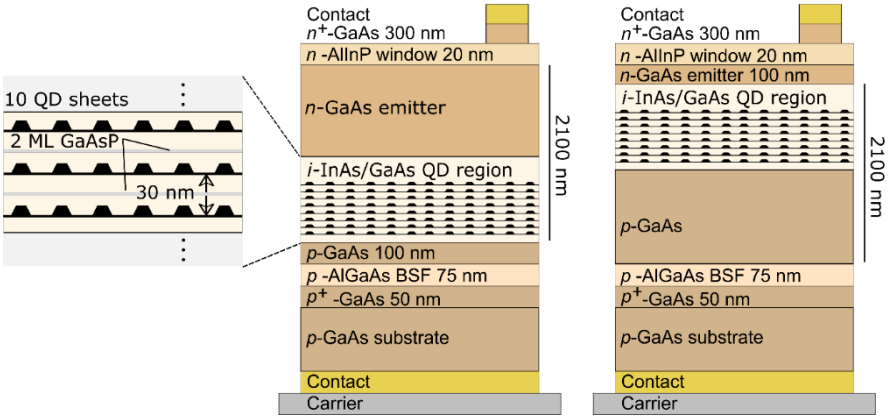

Fig. 11 The schematic layer structures for the deep (left) and shallow (right) junction InAs QD solar cells with the nominal layer thicknesses.

A set of samples was also grown in inverted manner to allow thin film processing and structures providing light management and photon recycling on the back and front surfaces.

The grown samples were processed to wafer based solar cells with size of 6×6 mm^2 by dicing and using a simple shadow mask process for forming front contact fingers. The backsides of the substrates were metallized as p-contacts.

Most of the cells were left without antireflection coating. The front contact finger pattern was formed using Ni/Au, and Ti/Au metallization was used for the bottom contacts. The contact metals were deposited by electron beam evaporation.

Optical emission properties were characterized using an automated Accent RPM2000 photoluminescence (PL) mapping tool with ~25 mW diode laser excitation at 785 nm. The PL emission was recorded either using a CCD detector array or an InGaAs photodiode array, depending on the emission wavelength. The symmetric GaAs(004) x-ray diffraction (XRD) Ω-2θ scans, to compare the crystal properties of DJ and SJ QD structures, were recorded using an X'Pert Pro MRD high resolution XRD system. Surface quality and QD density properties were investigated using light microscopy (Nikon L200) and atomic force microscopy (AFM) (Veeco DI3100 AFM system), respectively. The external quantum efficiencies (EQE) were measured in the wavelength range from 380 nm to 1100 nm using a self-made measurement system based on a 250 W QTH lamp (Oriel), a DK240 monochromator (Digikröm), appropriate long-pass and short-pass optical filters, and NIST calibrated Si and Ge reference photodiodes. The electrical parameters of the solar cells were deduced from light-biased current-voltage (*I–V*) measurements using an OAI TriSol solar simulator adjusted to AM1.5D conditions (the spectrum was normalized to 1000 W/m^2).

3.2.2 Photoluminescence characteristics

The room temperature PL of two sets of InAs QD cells are shown in Fig. 12. Fig. ***12***a shows the differences between luminescence properties of SJ and DJ InAs QDSCs and reference GaAs SC. The DJ cell emitting at slightly longer wavelength shows about one half of the emission intensity compared to the SJ structure The small emission wavelength difference for the SJ and DJ structures originates from slightly different deposition rates of indium during the growths on different days. There is also a clear intensity difference in the wetting layer emission at 920 nm between the two structures. This may imply a larger non radiative recombination of the photogenerated carriers in the DJ structure. The full-width-at-half-maximum values of the ground state emission peaks are ~64 nm and ~67 nm for SJ and DJ, respectively. The rather wide emission peak width indicates that either excited states take part to the emission or the broadness arises at least partially from QDs with different sizes.

In Fig. 12b, the PL spectra from InAs QDSCs with different number of QD layers are shown. We varied the number of InAs QD layers in a DJ structure from 5 to 20 to study the effects of the number of QD layers on the optical emission. The PL peak intensity increases roughly linearly with the number of QD layers indicating that at least from the optical emission point of view the QDs maintain their activity even with 20 QD layers. On the high energy side of the ground state PL peak one also observes a PL component from excited states or from a population of smaller sized QDs.

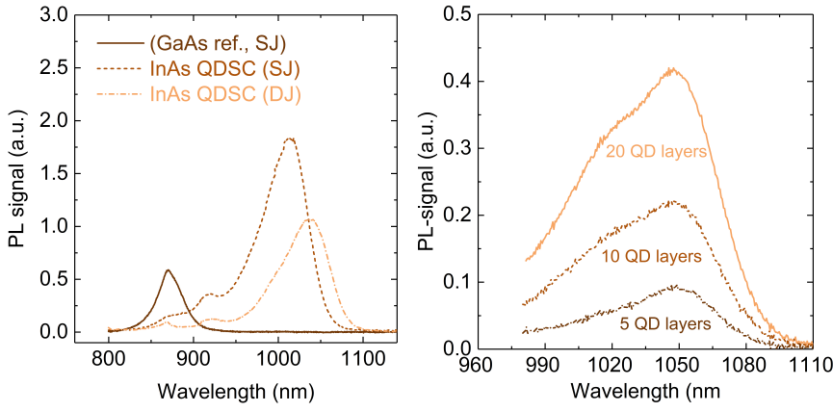

Fig. 12 (a) PL of GaAs, DJ and SJ InAs QDSCs. **(b)** PL from QDSCs with 5, 10 and 20 QD layers.

3.2.3 Surface characteristics

The InAs QD density was measured using AFM on samples that were separately grown on GaAs(100). Typically, the measured QD density in our samples was higher than $5x10^{10}$ cm^{-2}. For the growth conditions used in [100] the QD density was measured to be ~$7x10^{10}$ cm^{-2}. AFM images also indicated that the size distribution of the QDs at these growth conditions is at least bimodal, suggesting that there are different sizes of QD contributing to the photogeneration.

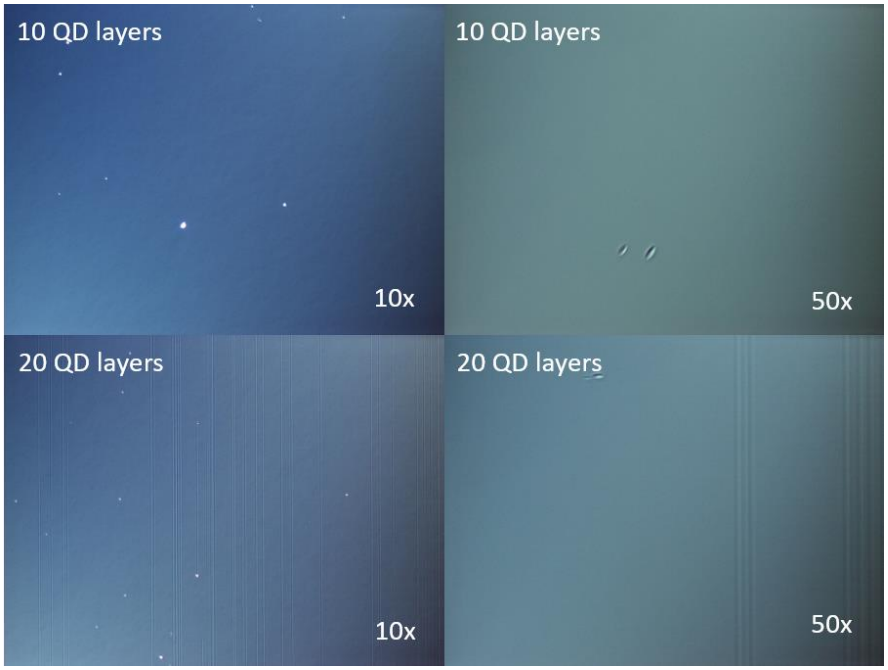

Fig. 13 Microscopy images for InAs QD solar cell structures with 10 and 20 QD layers.

The accumulation of strain in the InAs QD solar cells along the number of QD layers is also another concern. The consequence of not applying strain management is demonstrated in microscopy images shown in Fig. 13. The samples with 10 QD layers show only a few surface defects at magnifications of 10× and 50×, but otherwise the surface seems to be free of dislocation lines. For samples with 20 QD layers a number of dislocation lines have appeared already at 10× magnification, which indicates that for 20 InAs QD layers the accumulated compressive strain exceeds the threshold for dislocation formation.

Additionally, we find that the inter-QD-layer distance drastically affects the crystalline quality of the InAs QD solar cells – especially when no strain management is used. Fig. ***14*** demonstrates the effect of the inter-QD-layer distance on

surface morphology of the structures with 20 QD layers. For inter-QD-layer distances of 50 nm, no dislocation lines are visible at 10× magnification. However, when the inter-QD-layer distance becomes 30 nm or smaller, dislocation lines appear in microscopy images. For 30 nm inter-QD-layer distance, only a few lines are visible, but for 26 nm a dense dislocation line pattern is observed. Such observations are in line with earlier observations on multi-QD-layer structures in which the accumulating strain in one QD layer affects the growth of the next QD layer when the inter-QD-layer distance becomes too thin [120]. Therefore, to maintain pseudomorphic growth and keep the misfit dislocation line density at minimum, it is essential to manage the accumulating strain within the structures using tensile strained layers added to the structures.

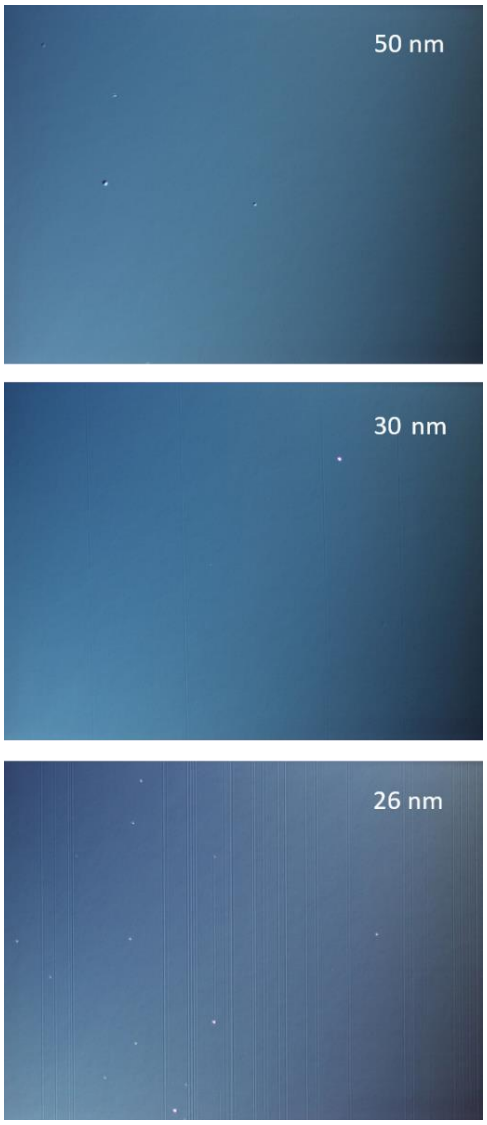

Fig. 14 Microscopy images (10 × magnification) taken from DJ InAs QD solar cell structures with different inter-QD-layer distances varying from 50 nm down to 26 nm.

We have adopted the strain management approach published by Hubbard's group on MOCVD-grown InAs/GaAs QD solar cells [33] in which a thin layer of GaAsP is grown inside the GaAs inter-QD-layer between the QD layers. To study the effects of insertion of GaAsP layers, XRD measurements are essential to determine

the grown structure. The fitting to the measured XRD patterns was done using a commercial dynamical diffraction theory-based software RADS Mercury [121].

Below, we shortly discuss the differences observed in XRD measurements between InAs QD solar cells with and without strain management. Fig. ***15*** compares typical symmetric Ω-2θ XRD scans taken over the GaAs (004) reflection on InAs QD solar cells with and without strain management. In the upper pane of Fig. 15, XRD of a solar cell structure without strain management is shown while in the lower pane the solar cell has thin GaAsP strain management layers inserted between the QD layers. Both structures show the main peak corresponding to GaAs (004) reflection and periodic satellite peaks on both sides of the main peak. The satellite peaks for the sample without strain management are slightly shifted towards compressive side of the main peak compared to the sample with strain management. This shift is related to the strain in the superlattice structure and can be used for further analysis of the effect of GaAsP layers used for strain management. In fact, one of the satellite peaks is masked by the GaAs (004) peak in the sample with strain management. Another difference between the samples can be seen on the right hand side of the GaAs (004) diffraction peak. For the strain-managed structure the periodic satellite peaks are higher and more of them are detected, especially on the tensile strain side of the GaAs (004) diffraction peak suggesting higher crystal quality. The main difference between the samples can be seen on the right hand side of the GaAs (004) diffraction peak. For the strain-managed structure the periodic satellite peaks are higher and more of them are detected, especially on the tensile strain side of the GaAs (004) diffraction peak. The inter-QD-layer distance can also be deduced from the distance of the superlattice (SL) satellite peaks in the XRD measurement graph using the relation $1/\Lambda = (2\sin(\theta_n)-2\sin(\theta_{n-1}))/\lambda$, where Λ is the period of the SL, θ_n and θ_{n-1} are the adjacent SL peak angles, and λ is the x-ray wavelength (1.54056 Å for Cu $K_{\alpha 1}$) [122].

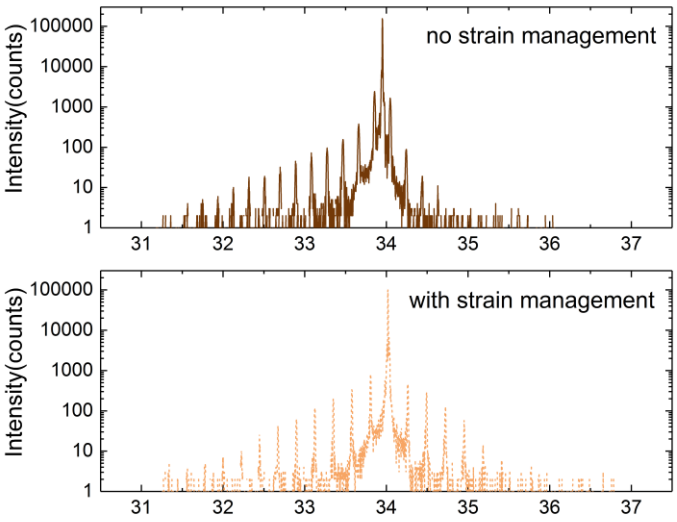

Fig. 15 Omega-2Theta XRD scans over the GaAs (004) reflection from InAs QD solar cells with (bottom) and without (top) GaAsP strain-management layers.

3.2.5 InAs/GaAs QD solar cell I–V characteristics

The room temperature I–V measurement results for best performing SJ and DJ solar cells are shown in Fig. 16. The electrical parameters of the best DJ and SJ InAs QD solar cells without antireflection coating are reported in Table 1. For the DJ structures there is an inverse linear relation between the V_{oc} and the number of QD layers. For zero layers, i.e. GaAs reference cell, the V_{oc} is 0.917 V, whereas for a cell with 20 QD layers V_{oc} is reduce to 0.852 V. The decrease of 2.5 mV per QD layer between 10 and 20 QD layers is close to 26 mV × ln(20/10), i.e. 1.8 mV per QD layer predicted in [40]. Our interpretation is that the origin of the reduction in the V_{oc} is most likely related to increased recombination in the QD region [100]. The SJ structures seem to work better in our case: for a wafer based GaAs reference cell V_{oc} of 0.979 V was obtained while an InAs QD cell with 10 QD layers exhibited V_{oc} of 0.94 V, which is only 0.39 mV less than for the GaAs reference cell. The small V_{oc} penalty upon insertion of the QD layers indicates that the quality of the InAs QD layers are very good. Also, the QD cells show slightly increased short circuit current densities for both DJ and SJ structures, which indicates that indeed there is an increased photocurrent from the QD layers.

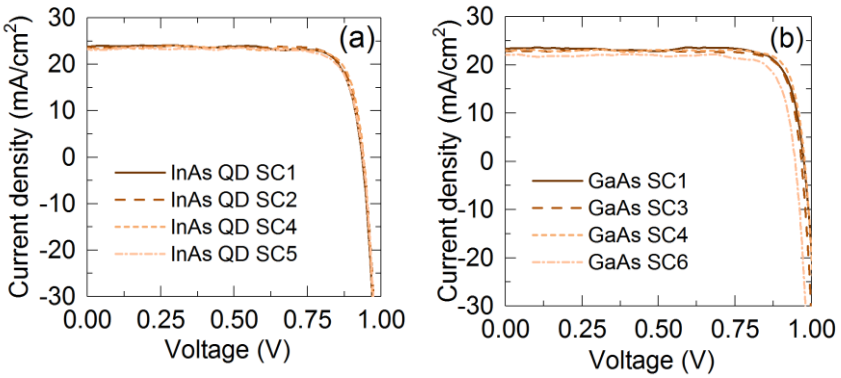

Fig. 16 (a) I–V for the four best wafer based SJ InAs QD SCs. (b) I–V for the four best wafer based SJ GaAs SCs.

Table 1 Electrical parameters of the best DJ and SJ solar cells [100].

Structural elements				Electrical parameters			
Material		QD layers	Junction type	V_{oc} (V)	J_{sc} (mA/cm^2)	FF (%)	Efficiency (%) (active area)
R2262	GaAs	0	DJ	0.917	19.5	80.2	14.3
R2272	InAs QD	10	DJ	0.877	22.6	81.7	16.2
R2270	InAs QD	20	DJ	0.852	21.9	79.2	14.8
R2275	GaAs	0	SJ	0.979	21.7	83.8	17.8
R2274	InAs QD	10	SJ	0.940	22.1	83.9	17.4

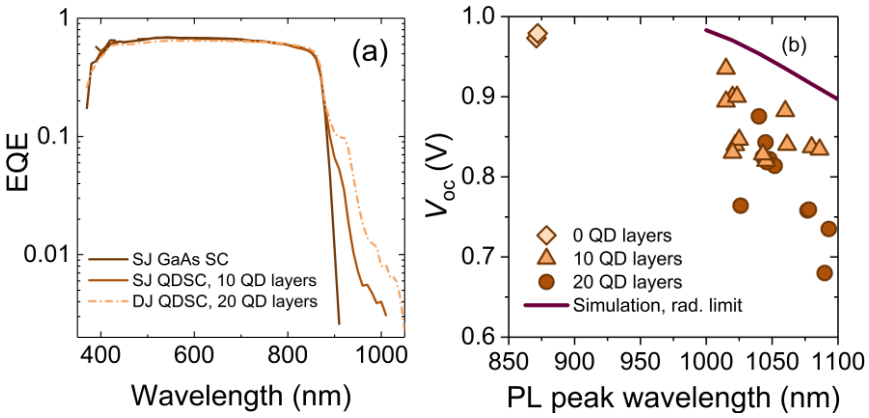

Fig. 17 (a) Examples of EQEs of the SJ GaAs and InAs QDSCs with 10 and 20 InAs QD layers. **(b)** V_{oc} values versus PL peak emission wavelength for wafer based GaAs and InAs QDSCs with either 10 or 20 QD layers. The simulated radiative limit for the V_{oc} is also shown as continuous line.

Most of the increased photocurrent of the wafer based cells originated from the thin InAs wetting layer. This can be seen in the EQEs of Fig. 17a, which shows that at the wavelengths corresponding to the wetting layer photogeneration, the EQE for 10 QD layers is about 7% whereas the contribution of the electronic states of the QD at longer wavelengths is marginal. For 20 QD layers the contribution of the wetting layer increases to 10% and those of the QD ground and excited states to the photogeneration become more visible.

Also, it was found, similarly to MOCVD-grown InAs QD solar cells [11], that there is an inverse relationship between the V_{oc} values and QD PL emission wavelength of the cells. In Fig. 17b the simulated V_{oc} under radiative limit for a solar cell with 10 QD layers is also drawn for comparison. The best obtained experimental V_{oc} values are ~ 40–60 mV below the calculated radiative limit. The experimental and simulated results indicate that, the larger an InAs QD gets, the deeper the associated potential well becomes, leading to higher recombination probability at the QD sites. A high V_{oc} can be obtained by reducing the QD size. The downside of this is that the decreased QD size also leads to decreased added photocurrent. To increase photogeneration in the QD layers one would thus need

to use higher number of QD layers, which again eventually would lead to reduced V_{oc}. To circumvent the problems arising from increasing the number of QD layers one shall use smart photon management within the structures to allow for higher absorption at the QD layers and higher photogeneration. The next section will concentrate on the photon management aspects of the thin-film InAs QDSCs.

4 Photon management approaches for high-efficiency thin-film III-V solar cells

Overcoming the weak optical absorption of QDs to compensate for the intrinsic V_{oc} loss is a mandatory path to demonstrate high efficiency QDSCs. The development of light trapping structures in QD solar cells involves two components: the fabrication of the back surface reflector and the structuring of the antireflection coating. With planar back surface reflectors, the optical length in absorptive layers can be effectively doubled. Furthermore, the optical length of the photons can be enhanced even more with diffractive gratings with reflector in the back surface of the solar cell. Diffractive gratings together with structured antireflection coatings (ARCs) create an optical system inducing photons to experience multiple round trips across the cell, increasing the absorption of light into the active layers.

In this section, we discuss the potential of light trapping enhanced QD cells based on the realistic device model introduced in Sec. 2.1, and the associated requirements in terms of QD current gain for the light trapping structures. ELO thin film cells with almost doubled photocurrent and preserved V_{oc} are demonstrated. Different planar reflectors and their suitability to be used in III-V solar cells are discussed. More specifically, we address the design and development of diffractive gratings and the development of structured antireflection coatings. Finally, the role of a micro-patterned rear contact design to optimize the photon-recycling effect is discussed.

4.1 Light trapping enhanced QD solar cells

The genuine thin film structure obtained by ELO is an excellent platform for the implementation of effective photon management strategies – as described in Sec. 5 - to maximize photon trapping and minimize reflection loss. Fig. ***18*** analyses the potential in terms of achievable short circuit current and efficiency of QDSCs with i) a wafer-based configuration; ii) a thin-film structure with planar rear mirror – double pass configuration; iii) a thin-film structure with textured rear surface – light trapping configuration.

The optical flux in the cell is described by an incoherent multiple reflection model [123, 124], as depicted in Fig. 18b, with

- R_f=0 and R_b=0 for the wafer-based configuration
- R_f=0 and arbitrary $0<R_b\leq1$ for the double-pass configuration
- R_f=1-(1-R_{ext})/n^2, n being the semiconductor refractive index and R_{ext} the reflectance at the illuminated surface; $0<R_b\leq1$ and angular independent for the Lambertian-like light trapping configuration. Here R_b is intended as an equivalent parameter modeling the reflectance of the specific textured structure implemented at the cell rear side.

We take as reference the epilayer structure exploited for the 50 × QD solar cell analysed in Sec. 3.1.2, with 10, 20, 50, or 100 QD layers uniformly distributed in the ≈ 1 µm thick undoped part of the emitter. The analysis is carried out by assuming radiative recombination only and neglecting photon recycling. Moreover, it is assumed that the power loss due to the cumulative effect of reflection and shadowing is limited to 5%.

Fig. ***18***c reports the QD short circuit current contribution as a function of the rear surface reflectivity. J_{QD} is estimated by integrating the EQE in the QD wavelength range ($\lambda > 880$ nm) over the AM1.5G solar spectrum. The light trapping (LT) scheme provides a remarkable increase of the QD current contribution compared to the wafer-based configuration ($R_b = 0$) and to the planar (double-pass) one. Defining the QD current gain, G_{QD}, as the ratio between J_{QD} at a certain value of R_b and the JQD provided by the wafer-based cell ($R_b = 0$), we find that the maximum achievable gain is about 9.3, 7, 4.5, and 3.4 for the 10×, 20×, 50×, 100× QD cells, respectively.

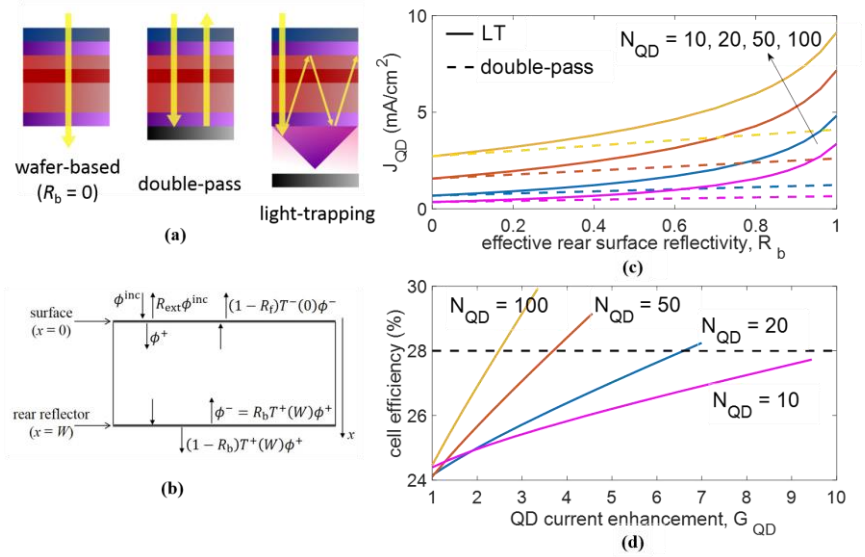

Fig. 18 (a) Basic InAs/GaAs QD solar cell structure implementing a single-pass configuration, double-pass configuration using a planar reflector, and full light trapping using a periodic diffraction grating and a reflector. **(b)** Conceptual scheme of light trapping. **(c)** QD current density as a function of the effective rear surface reflectivity for thin-film cell with planar mirror – double-pass configuration – and thin-film cell with textured mirror – light trapping configuration – using different numbers of QD layers. **(d)** Predicted cell efficiency as a function of the QD current enhancement with respect to the wafer-based configuration. The $R_b = 0$ point identifies the wafer-based configuration. Reprinted from Sol. Energy Mater. Sol. Cells, 181, F. Cappelluti et al., Light-trapping enhanced thin-film III-V quantum dot solar cells fabricated by epitaxial lift-off, pp.83-92, Copyright (2018), with permission from Elsevier.

The predicted power conversion efficiency as a function of G_{QD} is shown in Fig. 18d. It is worth noticing that when G_{QD}=1 – i.e. in the wafer-based cell – there is no practical advantage to increase the number of QD layers, because the J_{sc} increase produced by the QDs is barely sufficient – in the best case - to compensate for the intrinsic V_{oc} loss. Therefore, improvements in the QD growth – either in terms of layers or sheet density - must be combined with light trapping to achieve high efficiency. Similar considerations were drawn for IB-QDSCs [41] on the basis of detailed-balance calculations. A ten-fold or seven-fold increase of the QD current is demanded for thin-film 10× and 20× QD solar cells, as those investigated in this chapter, to approach 28% efficiency.

4.2 ELO QD cells with planar rear mirror

Fig. **19** shows a 3-in diameter thin-film QD GaAs solar cell structure that was processed into an array of individual 5x5 mm^2 solar cells. The structure containing 10 InAs QD layers was produced by MBE at Tampere University, ELO and thin-film cell processing was performed by Radboud University and tf2 devices. As a reference an equivalent structure was produced and processed while it remained on its native wafer (substrate-based cell).

Fig. **20** indicates that both cells suffer from a relatively small V_{oc} penalty in the range of 150-170 mV (as shown in Fig. 6 where GaAs cells without QDs have a V_{oc} of about 1.05 V). The V_{oc} penalty in the ELO cell is slightly larger (18 mV) but this difference is more than compensated for by the larger J_{sc} and fill-factor (FF) of the ELO cell as compared to the substrate-based cell resulting in an 0.4% higher cell efficiency. The EQE shown in

Fig. **20** shows that the increased J_{sc} of 0.7 mA/cm^2 results from an enhanced absorption in the wavelength range above the GaAs cut-off wavelength of 875 nm owing to the QD layers as well as in the wavelength range just below 875 nm owing to an enhanced photon confinement. The EL signal of the cells (insets in

Fig. **20**) does not reveal any apparent defects neither in the substrate-based nor in the thin-film cells.

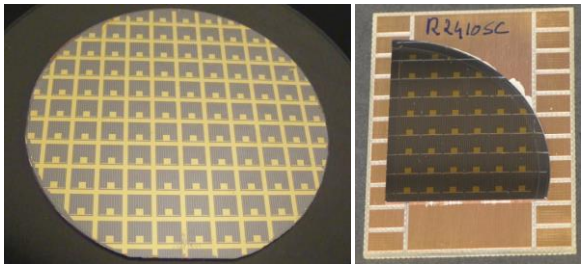

Fig. 19 Array of 5x5 mm^2 thin-film quantum dot (TFQD) solar cells, released from a 3-in diame-

ter GaAs wafer (left). Array of 5x5 mm^2 substrate-based quantum dot reference cells, on a section of a 3-in wafer (right).

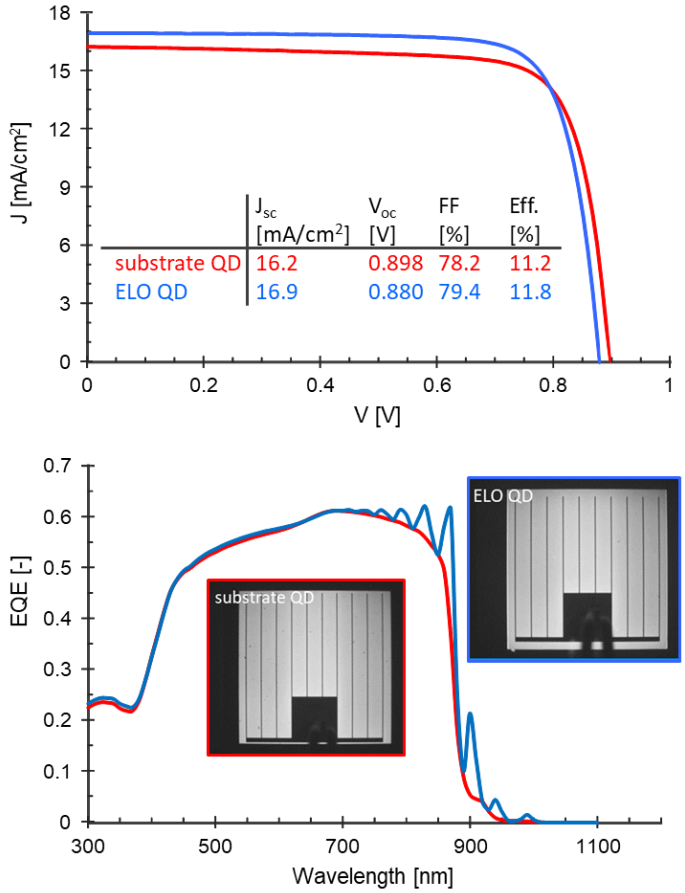

Fig. 20 J-V (upper figure), EQE (lower figure) and EL (insets) characteristics of 5x5 mm^2 ELO QD and substrate-based QD solar cells. Note that neither the ELO nor the substrate based cells were equipped with anti-reflection coatings.

4.3 Structures for photon management

4.3.1 Comparison of different metals for planar reflectors

Planar back surface reflectors such as Ag, Au, and Cu provide almost ideal reflectivity at wavelengths longer than 800 nm [125]. Au is known to be rather expensive material, and therefore the use of other highly conductive metals, such as Ag and Cu, would reduce the solar cell fabrication costs. Ag back reflectors have been demonstrated in III-V solar cells [126, 127] and Cu has also been used as a part of the back contact. However, Cu is known to diffuse into III-V semiconductors and thus to reduce the open circuit voltage (V_{oc}) of the solar cell [128–130]. This could be alleviated by applying a double-layer Ag/Cu reflector. The purpose of Ag is to act as a diffusion barrier for Cu and to provide high reflectance in combination with Cu layer. The Cu layer acts as a current spreader and conductor. In addition, Ni is required between the Au and Cu layers as an adhesion layer and Au acts as a protective layer and bonding surface.

The performance of planar back surface reflectors incorporating different metal layers were investigated with single-junction GaInNAs solar cells that were grown by MBE [7]. The metal reflectors were deposited using an electron beam evaporator and the samples details are given in Table I.

Table 2 Description of the fabricated samples

Back surface reflector	Metal layers	Thickness (nm)
Ti/Au	Ti/Au	50/100
Au	Au	100
Cu	Cu	100
10 nm Ag/Cu	Ag/Cu/Ni/Au	10/100/10/50
30 nm Ag/Cu	Ag/Cu/Ni/Au	30/100/10/50
50 nm Ag/Cu	Ag/Cu/Ni/Au	50/100/10/50

External quantum efficiency (EQE) results of the solar cells with different metal layers as back reflectors are presented in Fig. 21a. The optical properties of the reflectors were characterized by reflectance measurements. To this end double-side polished semi-insulating (SI) GaAs samples with back reflectors were used and the results are shown in Fig. 21b. Compared to conventional Ti/Au reference, the EQE was improved for the solar cells with Au, Ag/Cu, and Cu back reflectors. The greatest improvement in EQE was observed near the band edge of GaInNAs, where the absorption coefficient decreases and transmission increases –

we note that this situation resembles the behavior of QD solar cells, both in terms of wavelength range and low value of absorption. The highest EQE was obtained for the samples with Ag/Cu reflector, which could be the result of higher reflectance of the back reflector. This means that the photons that are not absorbed during the first pass are reflected back. The results between the 10 nm, 30 nm, and 50 nm Ag/Cu reflectors are identical, meaning that a 10 nm layer of Ag is already enough to preserve high reflectivity. Furthermore, thermal annealing had no impact on the EQE of the 10 nm Ag/Cu reflector, permitting the processing conditions at 200 °C [131].

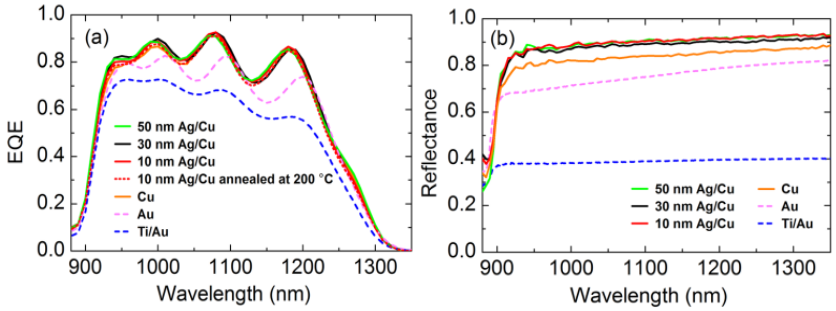

Fig. 21 (a) The EQE of the III-V solar cells with different back reflectors and **(b)** the reflectance of double-side polished SI-GaAs samples with back surface reflectors [131]. Reproduced from T. Aho et al., Enhancement of photocurrent in GaInNAs solar cells using Ag/Cu double-layer back reflector, Appl. Phys. Lett. 109, 251104 (2016), with the permission of AIP.

The current density (J_{sc}) values at AM1.5D (1000 W/m^2) spectral conditions [132] were calculated from the EQE results by integrating over the given spectrum and assuming a thick GaAs filter on top of GaInNAs cell. The results are collected in Table II. The solar cells with Ag/Cu reflectors exhibited J_{sc} values of ~14 mA/cm^2, which is more than 25% higher compared to the reference solar cell with Ti/Au reflector.

Back surface reflectors employed as ohmic contacts require a low contact resistivity. Conventional ohmic contacts are made of alloyed metals wherein annealing is shown to lower reflectivity due to the reduction of interface sharpness when compared to non-alloyed contacts [92]. On the other hand, non-alloyed contacts usually suffer from higher contact resistivity [133], yet high doping levels can be employed in the contact GaAs layer to reach low contact resistivity values [128]. Typically, contact resistivity values for p-GaAs are of the order of 10^{-5} Ω·cm^2 and 10^{-7} Ω·cm^2 for non-alloyed and for alloyed metal contacts, respectively [133, 134]. The contact resistivity obtained for the different non-alloyed layers used in our study deposited on a p-type GaAs layer with a doping level of ~10^{20} cm^{-3} are presented in Table II; the measurements were made using the Transmission Line Method (TLM). As presented in Table II, all the reflectors showed low contact resistivity of the order of 10^{-6} Ω·cm^2, which are lower than reported con-

tact resistivity values of non-alloyed contacts [134]. These results show that an ohmic contact is formed even without annealing due to high doping in the GaAs layer and high reflectivity of the metal reflector is retained. In addition, the Ag/Cu reflector had good adhesion to III-V semiconductor and a thin Ag layer acts as a diffusion barrier, preventing Cu diffusion into semiconductor structure even when the cell is subjected to thermal annealing [131].

Table 3 Measured contact resistivity results and J_{sc} values at AM 1.5D [131].

Back surface reflector	Contact resistivity ($\Omega \cdot cm^2$)	J_{sc} (mA/cm^2)
Ti/Au	3×10^{-6}	10.7
Au	1×10^{-6}	12.4
Cu	4×10^{-6}	13.4
10 nm Au/Cu	4×10^{-6}	13.6
10 nm Ag/Cu*	-	13.3
30 nm Ag/Cu	4×10^{-6}	13.7
50 nm Ag/Cu	5×10^{-6}	13.7

*Annealed at 200 °C for 90 s

4.3.2 Gratings for light diffraction in InAs/GaAs QDSC

Periodically textured reflectors patterned on the cell rear side can be exploited to enhance the QD absorptivity. ELO thin-film QD cells with textured back surface reflectors were reported in [42], demonstrating a 30% increase of QD current contribution compared to a cell with planar reflector. Effective light trapping by back side periodic grooves has also been demonstrated in multiple quantum well solar cells in [135], attaining a fivefold increase of the sub-bandgap optical path length.

Here, we report the design and experimental development of diffractive rear mirrors for thin-film QD cells. These structures are designed with a period larger than the incident wavelength, so that the reflector excites high order diffractive modes that propagate outside the escape cone and get reflected multiple times through the absorber material.

Possible designs with uni-periodic gratings with triangular cross-section and bi-periodic pyramidal gratings directly imprinted on the widegap (AlInP) back surface field layer are shown in Fig. 22. A planarizing polymer layer (SU-8) is used to alleviate the parasitic losses due to unwanted surface plasmon effect that could arise at the large interface between the microstructured semiconductor and the metallic (Ag) mirror [136, 137]. The planar ARC can be composed of several materials, including a single layer of Si_3N_4, or a double layer of SiO_2 and TiO_2. Alternatively, a nanostructured pyramidal ARC could be patterned directly on the AlInP window layer [138].

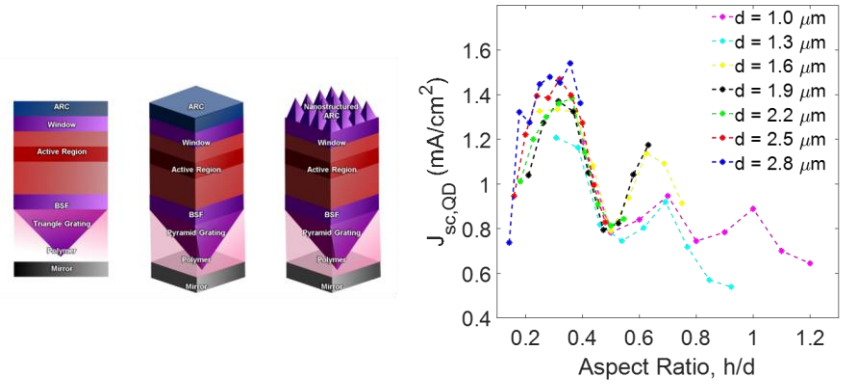

Fig. 22 (a) Sketch of thin-film solar cells integrating: planar ARC and triangular grating; planar ARC and pyramidal grating; nanostructured ARC and pyramidal grating. The active region is composed of GaAs emitter, a stack of 10 InAs/GaAs QD layers, and GaAs base. **(b)** QD short-circuit current contribution as a function of the aspect ratio for a uni-periodic triangular grating without metallic reflector. Adapted with permission from [139] © The Optical Society.

The structures were simulated with the Rigorous Coupled-Wave Analysis (RCWA) method [140] in order to identify the grating configuration that maximizes the QD current contribution, $J_{sc,QD}$. This is estimated integrating over the QD wavelength range the absorbed photon density in the active region. As seen in Fig. 22b, it turns out that the most relevant design parameter is the height/period aspect ratio of the grating, with optimum values between 0.32 and 0.38. The same optimum was also found for gratings realized in low index materials [141].

Fig. **23** shows examples of calculated absorbance spectra for cells with a pyramidal grating with height of 900 nm and period of 2400 nm, exploiting a planar ARC and a nanostructured AlInP ARC, respectively. For reference, also the absorbance of an unpatterned cell (equivalent to a wafer-based configuration) and of a cell with planar reflector and ARC are shown. The enhancement due to light trapping is evident close to the GaAs band gap and in the QD absorption region (λ = 890 – 1200 nm). From these spectra, we estimate that the cell with planar ARC and pyramidal backside grating provides a photocurrent increase of 16 times with respect to the unpatterned cell. In the double-side patterned cell, the combined action of the front ARC and backside diffraction grating provides more effective light trapping with a current increase of about 27. Such values are very promising when compared to the needs in terms of QD current gain set in Fig. 18 to surpass the 28% target efficiency.

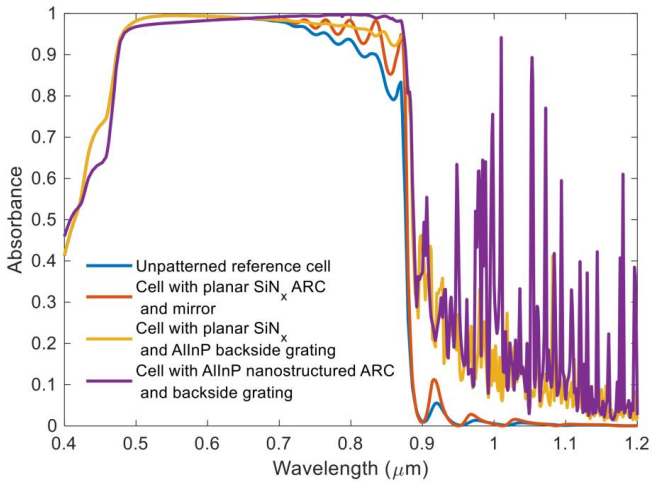

Fig. 23 Absorbance comparison between the planar reference cell, cell with planar ARC with mirror, cell with planar ARC and back-side grating, cell with nano ARC and back-side grating. Adapted with permission from [142] © The Optical Society .

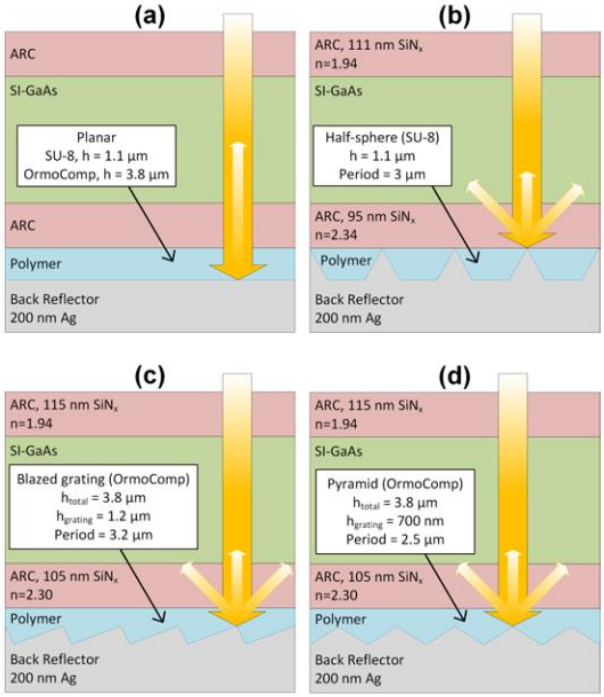

Fig. 24 The schematic drawing of the diffraction structures, **(a)** planar, **(b)** half-sphere grating, **(c)** blazed grating and **(d)** pyramidal grating. Reprinted with permission from [143] © The Optical Society.

Diffraction gratings test structures with the optimum aspect/ratio of 0.32–0.38, were fabricated using a double-side polished SI-GaAs substrate which was embedded with single-layer SiN_x antireflection coatings. The ARC thicknesses and refractive indexes are presented in Fig. 24, which introduces the three investigated geometries, namely halfsphere, blazed, and pyramid gratings, and the planar reference.

The half-sphere gratings were fabricated by photolithography using a commercial epoxy based negative photoresist, SU-8 (MicroChem Corp.), which is commonly used in the electronic industry. To obtain the desired half-sphere structure, photolithography process parameters such as spin coating speed, exposure time, and baking temperatures were optimized. For blazed grating and pyramidal grating, a commercial OrmoComp nanoimprint lithography (NIL) photoresist (Micro Resist Technology GmbH) was used in the NIL processes. The gratings were transferred from NIL master into the NIL photoresist. Fig. ***25*** shows the detailed images of the three experimental structures. The top of the half-sphere appeared slightly flattened, as shown in the optical profilometer measurement in Fig. 25a. The scanning electron microscopy (SEM) images of the pyramid grating, presented in Fig. 25c and Fig. 25d, are taken from the back surface of the sample where 200 nm Ag is evaporated, whereas the blazed grating image in Fig. 25b is the cross-section of the polymer grating without Ag.

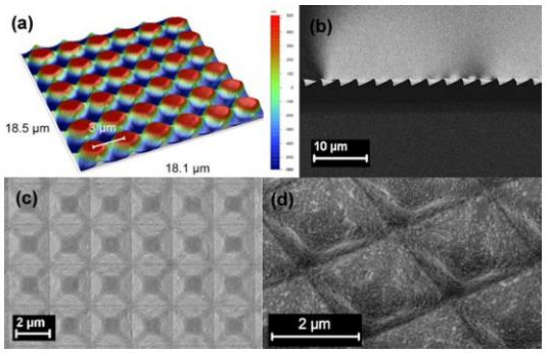

Fig. 25 (a) Optical profilometer image of the half-sphere structure, **(b)** SEM-image of the blazed grating, **(c)** and **(d)** SEM image of the pyramidal grating. Reprinted with permission from [143] © The Optical Society.

The specular reflectance at 8° incident angle and the total reflectance were measured with spectrophotometer. All the measurements were carried out through the SI-GaAs wafer and the performance of the back reflectors were evaluated at the wavelengths for which SI-GaAs is transparent. The reflectance results of the half-sphere grating are presented in Fig. 26 (left), where the difference be-

tween the total and the specular reflectance represents the diffuse reflectance. A local maximum in the specular reflectance of the half-sphere is observed, decreasing the diffuse reflectance at the wavelength range of 950–1150 nm. The reflectance results of the blazed grating and the pyramid grating are compared in Fig. 26 (right). According to the results, the pyramid grating shows the highest diffuse reflectance when compared to the blazed grating or the half-sphere structure. In addition, the total reflectance of the blazed grating was lower compared to the pyramid grating, revealing some extra losses in the structure, probably originating from the surface plasmon resonance (SPR) in the metal reflector.

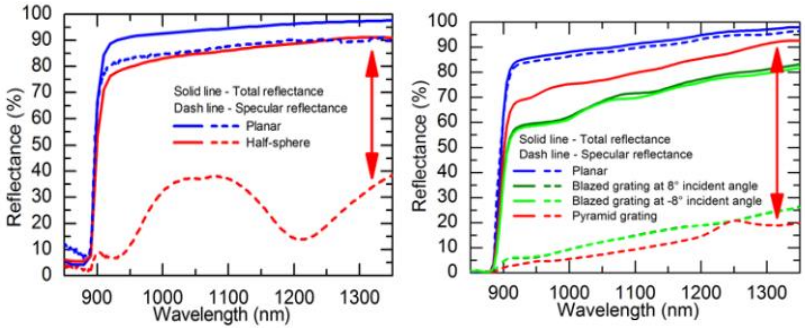

Fig. 26 Left: Total and specular reflectance of the half-sphere grating and the planar reference. Right: the blazed grating, pyramidal grating, and planar reference. Reprinted with permission from [143] © The Optical Society.

In order to understand the suitability of polymer grating architectures for space applications, an electron irradiation (1 MeV) study was performed to the samples with the Ormocomp polymer gratings. The reflectance spectra were measured after the electron irradiation. The reflectance results of the irradiated samples were identical up to doses of 1×10^{15} e^-/cm^2 when compared to the sample without irradiation in Fig. 26 (right), indicating that the polymer could be suitable for diffractive gratings in space solar cells.

4.3.3 Antireflection coatings using nano-gratings

To fully exploit light trapping in QD solar cells, nanostructured ARCs need to be considered. Tommila et al. have demonstrated NIL process to fabricate nanocones into AlInP window layer with the period of 300 nm [*138*]. The reflectance results of the nanocone ARC are presented in Fig. 27, where the red line is 300 nm period cone and the black line is the reference sample without any structuring. The 300 nm cone structure resulted in less than 5% average reflectance in the wide wavelength range of 400–1300 nm. As observed in the SEM image of the cone structure, presented in Fig. 27, the grating showed high uniformity.

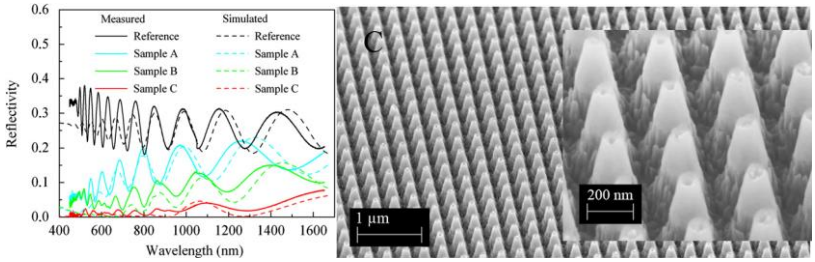

Fig. 27 Left: Simulated and measured reflectivity results of 300 nm period cones in AlInP (red line). Right: SEM images of 300 nm period cones [138]. Reprinted from Solar Energy Mater. Solar Cells, 94, J. Tommila et al., Nanostructured broadband antireflection coatings on AlInP fabricated by nanoimprint lithography, pp. 1845-1848, Copyright (2010), with permission from Elsevier.

To produce nanocone structures with smaller period (< 300 nm), a process simpler than the 300 nm cones process was devised and utilized. Based on simulations (not reported here), gratings with a period of 180 nm can be designed to achieve comparable reflectance lowering the height of the cones. This simplifies the processing of the nanocones. The SEM images of AlInP cones with the period of 180 nm are presented in Fig. 28. In addition, 40 nm SiN_x layer with refractive index of 2.0 was evaporated on top of the cones to further lower the reflectance.

The reflectance results to the samples before and after the SiN_x evaporation are presented in Fig. 29. The results show that the reflectance remains less than 5% from wavelength of 320 nm to ~950 nm for the sample without SiN_x layer and to ~1000 nm for the sample with SiN_x layer. The SiN_x layer on top of the AlInP cones shifts the peak to the longer wavelengths. As a reference, a GaAs solar cell with SiO_2/TiO_2 ARC is also presented in Fig. 29. The 180 nm cones have rough surface on top of the cones (Fig. 28), which might have an effect on the optical properties of the ARC. The rough top surface could possibly be avoided with the optimization of the etching process of the cones.

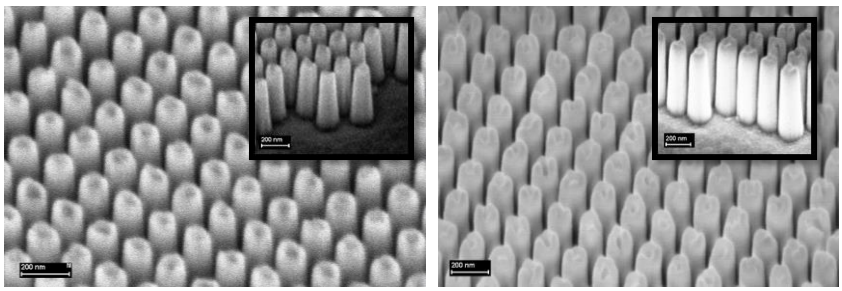

Fig. 28 (a) SEM images of 180 nm period cone structure in AlInP, **(b)** 40 nm SiN_x layer of top of the AlInP cones.

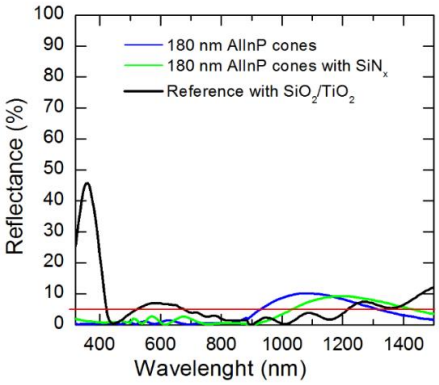

Fig. 29 Reflectance results of 180 nm AlInP cone structure. The red line represents the 5 % reflectance.

4.3.4 Patterned rear mirror/contact for enhanced photon confinement and recycling

For solar cells where the non-radiative recombination is sufficiently reduced, radiative recombination becomes the dominant loss mechanism. The performance of cells operating in this regime can be strongly enhanced by utilising the mechanism of photon recycling. Whereas in wafer based cells a large part of the regenerated photons might escape to the substrate, the back-contact geometry of a thin-film cell can be designed to optimize its reflectivity and maximally benefit from photon recycling [14, 16, 86, 94, 95, 144]. Fig. **30** shows the results of an approach in which the initially fully metalized back-contact of a single junction GaAs cell is reduced to a discrete number of contact points. In between the highly doped GaAs contact layer of the cell is etched away and replaced by a dielectric (ZnS) layer. In combination with the Au coated copper carrier the ZnS layer yields a strongly increased rear-side reflectivity (R) from 63.5% to 96.5% in the relevant wavelength range (840-870 nm) [145]. Therefore, by reducing the size of the rear contact points the fraction of the rear-contact surface coverage (Cr) also decreases resulting in an increased reflectivity from R = 63.5% for Cr = 100% up to R = 93.2% for Cr =10%. Fig. **31**a shows a 2-in diameter thin-film single junction GaAs cell structure that was processed into multiple individual 5x5 mm^2 solar cells with a different rear contact coverage in each quadrant. The EL signal of the cells (Fig. 31) does not reveal any apparent defect in the thin-film cells but clearly shows the decreasing size of the rear contact points. For the ease of contacting, the cells have a large front coverage of 16.6% which is about 10 times larger than that applied in our record cells [92]. Nevertheless, I-V analysis shows that the cells have efficiencies around 22% which corresponds to well over 25% in case a low coverage grid would be applied.

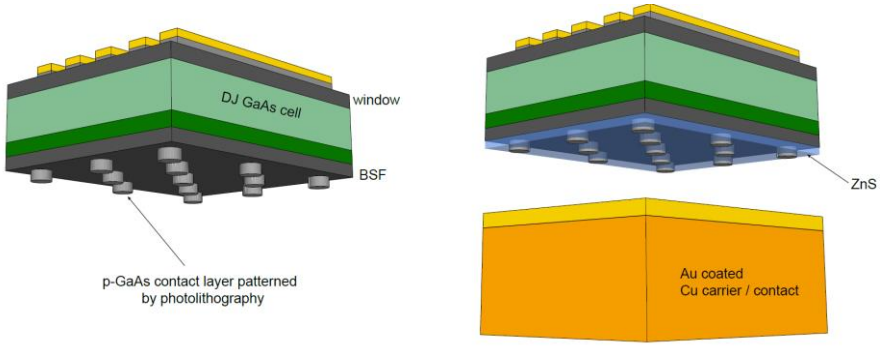

Fig. 30 Schematic representation (not to scale) of a partial contact approach to optimize the rear-side reflectivity of a III-V thin-film cell.

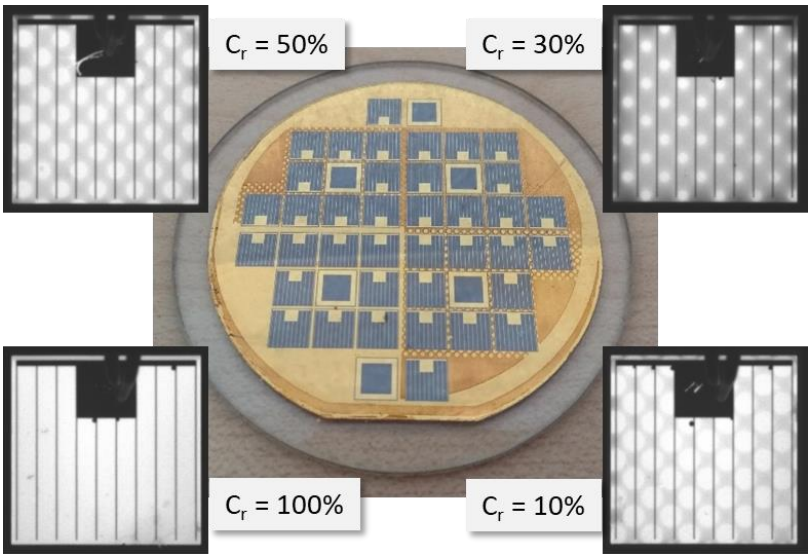

Fig. 31 2-in diameter thin-film GaAs cell structure containing multiple 5x5mm^2 solar cells with a different rear contact coverage (Cr) in each quadrant with the electroluminescence image of a cell from each section.

Related to the increasing distance between the rear contact points, the series resistance of the cells increases with decreasing Cr. As a result the fill-factor of the cells initially decreases gradually with decreasing Cr and later quite abruptly for Cr = 10%. On the other hand, decreasing Cr results in an increased rear-side reflectivity which according a theoretical study by Miller et al [16] should result in a linear increase in short circuit current density and a more than linear increase in open circuit voltage. Fig. **32** shows that the experimentally determined trend in J_{sc}

and V_{oc} confirm the theoretical predictions. The increased J_{sc} with R is simply the result of the increased reflection and subsequent absorption of photons in the active layers of the cell. On the other hand, the more than linear increase in V_{oc} with R is indicative for effective photon recycling in the solar cell. In follow-up experiments the rear-side reflectivity of the cell was increased from 93.2% to 96% by further decreasing the diameter of the rear contact points to 40 μm while at the same time their mutual distance was decreased to minimize resistive losses and maintain a high fill-factor. The V_{oc} of these cells was found to be 1.071 V providing further evidence for the rapid increase in cell voltage as the reflectivity approaches 100%. The present world record thin-film GaAs solar cell was reported to have a V_{oc} of 1.1272 V and a fill-factor of 0.867 [1]. Although the exact structure of this cell is not published, the high V_{oc} and fill-factor values suggest a DJ geometry with a near perfect back reflector.

In a more recent study [*146*] a highly doped AlGaAs back contact layer was applied which between the localized contact points was not fully not removed but partially etched using a NaOH/H2O2 solution. The induced surface roughness facilitated the application of a diffusive back-reflector which allowed for a strong reduction of the solar cell thickness. Due to the increased photon confinement, ultra-thin (300 nm) GaAs cells with such textured mirrors were demonstrated to have a highly increased current density yielding efficiency up to 21.4% whereas the efficiency in ultra-thin cells with planar mirrors was limited to 18.5%.

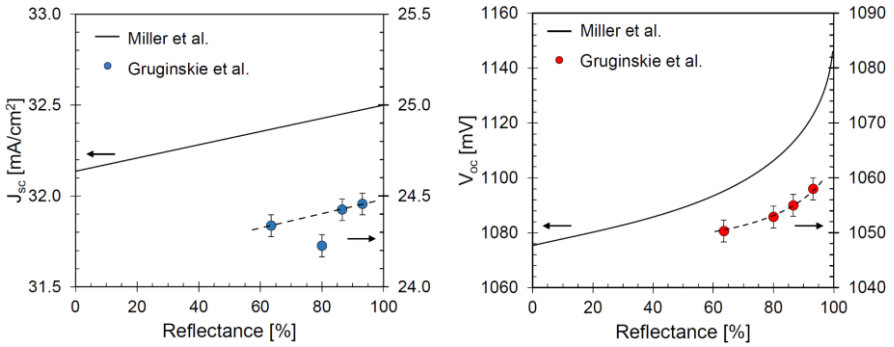

Fig. 32 Theoretically predicted [16] and experimentally determined [145] J_{sc} and V_{oc} as a function of the rear-side reflectivity in thin-film GaAs cells. Note that the J_{sc} values resulting from theory are significantly higher since the reflection of light at the ARC and grid contacts of the cell are neglected. Moreover, in the theoretical study, the total absence of non-radiative recombination is assumed.

5 Summary and outlook

Thin film III-V cells combined with light management structures are a very promising concept as alternative to the costly multi-junction cell route, both for space

and terrestrial uses. QDs may provide additional advantages such as higher radiation hardness in space and better matching to the sun spectrum in CPV, provided that the issues of large V_{oc} reduction and small QD photogeneration are solved.

In this contribution we have analysed the V_{oc} reduction due to intrinsic and extrinsic mechanisms. Intrinsic loss causes a linear dependence of the V_{oc} with the QD emission wavelength as verified experimentally by a large set of fabricated samples and theoretically by quantum-corrected drift-diffusion simulations. MBE grown 10× InAs/GaAs QD solar cells with high in-plane density QDs demonstrate V_{oc} higher than 0.95 V, a record value for MBE grown QDSCs, in line with record MOCVD grown QDSCs.

Numerical simulations demonstrate that light management is essential to improve the QD absorption and the cell efficiency. Incidentally, our study evidences that increasing the number of QD layers or the QD areal density is useful to achieve high efficiency QDSCs only if combined with light trapping. Towards this goal, successful ELO of MBE grown layer structures from 3-in wafers is reported. ELO QDSCs show a two-fold increase of the QD photocurrent and a high V_{oc} of 0.88 V, the highest ever reported for thin-film III-V QD cells. Several photon management structures have been discussed. A planar double-layer Ag/Cu back contact reflector - withstanding annealing temperatures of at least 200 °C - was demonstrated, resulting in 28% higher calculated J_{sc} than that of the reference Ti/Au back contact and low contact resistivity. Back reflector structures enabling light diffraction were designed and developed by employing different geometries. Efficient diffraction of light is observed for all the structures, indicating potential for improving the absorption and hence the current generation in the thin-film solar cells. Pyramid gratings showed the highest diffuse reflectance in the wavelengths corresponding to the photogeneration in InAs/GaAs QDSCs. The nanostructured ARCs fabricated into AlInP window layer showed less than 5% reflectance in the wavelength range of 400–1300 nm. These ARC nanostructures together with diffraction back surface reflectors will enable light trapping in QDSCs. The fabrication techniques of the light trapping structures are applicable also to other types of III-V solar cells by adjusting the dimensions of the gratings to be optimal for the specific wavelength range.

As the quality of the QD solar cell structures approaches that of regular solar cells, ELO QD cells can achieve higher V_{oc} than their substrate based counterparts by utilizing the photon confinement and recycling mechanisms, as already demonstrated in conventional single-junction cells. A novel rear contact/mirror design aimed at optimizing photon-recycling has been reported. A selective patterning technique of the bottom contact layer implemented in thin-film GaAs cells yields a clear non linear increase of V_{oc} well correlated to the increase of reflectance as the contact layer coverage is reduced from 100% to 10%. In addition, application of a diffusive rear-mirror was demonstrated to significantly increase the current density and efficiency of ultra-thin GaAs cells with an active layer thickness of only 300 nm.

The promising experimental results and the guidelines provided by the numerical simulations presented in this work demonstrate that high efficiency QD-based single- and multi-junction cells are feasible in the next future. In the longer

term, the achieved high material quality and V_{oc}, and the technology of photonic structures for light trapping and photon recycling will be instrumental to overcome the challenges posed by the implementation of intermediate band QDSCs.

Based on its efficiency improvements, III-V-based photovoltaic technologies have good prospects for a stepwise expansion from the current niche application areas. With the present wafer-based production technologies this might gradually proceed via CPV applications in areas with lower DNI. However, once the III-V photovoltaics industry succeeds in maturing the cost effective ELO production technology for genuine thin-film devices from reusable wafers, the cost of III-V space solar cells can drop significantly, while their power-to-weight ratio can increase substantially. Both factors will ease the realisation of satellite constellations. More importantly, it would enable CPV to become competitive in areas with much lower DNI, thereby substantially expanding the CPV and III-V photovoltaics markets. The utilization of III-V cells might then be further accelerated by the access of new market segments as well. Such markets might include Unmanned Aerial Vehicles [147, 148], motor vehicles [149] and portable electronics [147]. For ultimate large scale application in non-concentrating III-V solar modules in the build environment, besides ELO, a low-cost deposition technology is required for the production of the cell structures. Despite the huge challenges, developments are already being made in this direction [150].

Acknowledgments

The work was partly funded by European Union Horizon 2020 projects TFQD (Grant Agreement No. 687253) and ERC AdG project AMETIST (Grant Agreement No. ERC-2015-AdG 695116). The authors would also like to thank Dr. Arto Aho for valuable discussions, Dr. Jari Lyytikäinen and Mr. Eero Halonen for MBE related actions, and Ms. Marianna Raappana and Mrs. Ninja Kajas for sample processing support. The authors would also like to thank Prof. Huiyun Liu for his help with starting the QD growths.

References

1. Green, M.A., Emery, K., Hishikawa, Y., Warta, W., Dunlop, E.D.: Solar cell efficiency tables (Version 45). Progress Photovolt.: Res. Appl. **23**, 1-9 (2015)
2. Shockley, W., Queisser, H.J.: Detailed balance limit of efficiency of p- n junction solar cells. J. Appl. Phys. **32**, 510-519 (1961)
3. Jackson, E.D.: Transactions of the Conference on the Use of Solar Energy. Tucson, AZ, 122-126 (1955)
4. Ekins-Daukes, N.J.: III- V Solar Cells. Solar Cell Materials, 113-143 (2014)
5. Marti, A., Araújo, G.L.: Limiting efficiencies for photovoltaic energy conversion in multigap systems. Sol. Energy Mater. Sol. Cells **43**, 203-222 (1996)

6. Brown, A.S., Green, M.A.,: Limiting efficiency for current- constrained two- terminal tandem cell stacks. Progress Photovolt.: Res. Appl. **10**, 299-307 (2002)
7. Dimroth, F., Kurtz, S.: High-efficiency multijunction solar cells. MRS bulletin **32**, 230-235 (2007)
8. Dimroth, F., Tibbits, T.N., Niemeyer, M., Predan, F., Beutel, P., Karcher, C., Oliva, E., Siefer, G., Lackner, D., Fuß-Kailuweit, P., Bett, A.W.: Four-junction wafer-bonded concentrator solar cells. IEEE J. Photovolt. **6**, 343-349 (2015)
9. Philipps, S.P., Bett, A.W., Horowitz, K., Kurtz, S.: Current status of concentrator photovoltaic (CPV) technology (No. NREL/TP-5J00-65130). National Renewable Energy Lab (NREL), Golden, CO (United States) (2015)
10. Branker, K., Pathak, M.J.M., Pearce, J.M.: A review of solar photovoltaic levelized cost of electricity. Renewable and sustainable energy reviews **15**, 4470-4482 (2011)
11. Tanabe, K., Guimard, D., Bordel, D., Arakawa, Y.: High-efficiency InAs/GaAs quantum dot solar cells by metalorganic chemical vapor deposition. Appl. Phys. Lett. , **100**, 193905 (2012)
12. Tatavarti, R., Hillier, G., Dzankovic, A., Martin, G., Tuminello, F., Navaratnarajah, R., Du, G., Vu, D.P., Pan, N.: Lightweight, low cost GaAs solar cells on 4″ epitaxial liftoff (ELO) wafers. In 2008 33rd IEEE Photovoltaic Specialists Conference, 1-4 (2008)
13. Bauhuis, G.J., Mulder, P., Haverkamp, E.J., Schermer, J.J., Bongers, E., Oomen, G., Köstler, W., Strobl, G.: Wafer reuse for repeated growth of III–V solar cells. Progress Photovolt.: Res. Appl. **18**, 155-159 (2010)
14. Kayes, B.M., Nie, H., Twist, R., Spruytte, S.G., Reinhardt, F., Kizilyalli, I.C., Higashi, G.S.: 27.6% conversion efficiency, a new record for single-junction solar cells under 1 sun illumination. In 2011 37th IEEE Photovoltaic Specialists Conference, 4-8 (2011)
15. Lush, G., Lundstrom, M.: Thin film approaches for high-efficiency III–V cells. Solar cells **30**, 337-344 (1991)
16. Miller, O.D., Yablonovitch, E., Kurtz, S.R.: Strong internal and external luminescence as solar cells approach the Shockley–Queisser limit. IEEE J. Photovolt. **2**, 303-311 (2012)
17. Wang, X., Khan, M.R., Gray, J.L., Alam, M.A., Lundstrom, M.S.: Design of GaAs solar cells operating close to the Shockley–Queisser limit. IEEE J. Photovolt. **3**, 737-744 (2013)
18. National Renewable Energy Laboratory (NREL): Low-Cost III-V Solar Cells, <https://www.nrel.gov/pv/low-cost-iii-v-solar-cells.html>
19. Kurtz, S.R., Olson, J.M., Faine, P.: The difference between standard and average efficiencies of multijunction compared with single-junction concentrator cells. Solar Cells **30**, 501-513 (1991)
20. Warmann, E. C., Atwater, H. A.: Energy production advantage of independent subcell connection for multijunction photovoltaics. Energy Science & Engineering **4**, 235-244 (2016)
21. Villa, J., Martí, A.: Impact of the spectrum in the annual energy production of multijunction solar cells. IEEE J. Photovolt. **7**, 1479-1484 (2017)
22. Warren, E. L., Deceglie, M. G., Rienäcker, M., Peibst, R., Tamboli, A. C., Stradins, P.: Maximizing tandem solar cell power extraction using a three-terminal design. Sustainable Energy & Fuels **2**, 1141-1147 (2018)
23. Linares, P. G., Antolín, E., Martí, A.: Novel heterojunction bipolar transistor architectures for the practical implementation of high-efficiency three-terminal solar cells. Sol. Energy Mater. Sol. Cells **194**, 54-61 (2019)

24. Barnham, K. W. J., Ballard, I., Connolly, J. P., Ekins-Daukes, N. J., Kluftinger, B. G., Nelson, J., Rohr, C.: Quantum well solar cells. Physica E: Low-dimensional Systems and Nanostructures **14**, 27-36 (2002)
25. Aroutiounian, V., Petrosyan, S., Khachatryan, A., Touryan, K.: Quantum dot solar cells. J. Appl. Phys. **89**, 2268-2271 (2001)
26. Hubbard, S., Bailey, C., Polly, S., Cress, C. D., Andersen, J., Forbes, D. V., Raffaelle, R. P.: Nanostructured photovoltaics for space power. Journal of Nanophotonics **3**, 031880 (2009)
27. Lumb, M. P., Dobbin, A. L., Bushnell, D. B., Lee, K. H., Tibbits, T. N. D.: Comparing the energy yield of (III–V) multi- junction cells with different numbers of sub- cells. In AIP Conference Proceedings **1277**, 299-302 (2010)
28. Welser, R. E., Sood, A. K., Laghumavarapu, R. B., Huffaker, D. L., Wilt, D. M., Dhar, N. K., Sablon, K. A.: The physics of high-efficiency thin-film III-V solar cells. In Solar Cells-New Approaches and Reviews. IntechOpen. (2015)
29. Luque, A., Martí, A.: Increasing the efficiency of ideal solar cells by photon induced transitions at intermediate levels. Phys. Rev. Lett. **78**, 5014 (1997)
30. Luque, A., Martí, A.: The intermediate band solar cell: progress toward the realization of an attractive concept. Advanced Materials **22**, 160-174 (2010)
31. Okada, Y., Ekins-Daukes, N.J., Kita, T., Tamaki, R., Yoshida, M., Pusch, A., Hess, O., Phillips, C.C., Farrell, D.J., Yoshida, K., Ahsan, N.: Intermediate band solar cells: Recent progress and future directions. Applied physics reviews **2**, 021302 (2015)
32. Sakamoto, K., Kondo, Y., Uchida, K., Yamaguchi, K.: Quantum-dot density dependence of power conversion efficiency of intermediate-band solar cells. J. Appl. Phys. **112**, 124515 (2012)
33. Hubbard, S.M., Cress, C.D., Bailey, C.G., Raffaelle, R.P., Bailey, S.G., Wilt, D.M.: Effect of strain compensation on quantum dot enhanced GaAs solar cells. Appl. Phys. Lett. **92**, 123512 (2008)
34. D. Zhou, G. Sharma, S. Thomassen, T. Reenaas, B. Fimland, Optimization towards high density quantum dots for intermediate band solar cells grown by molecular beam epitaxy, Appl. Phys. Lett. **96**, 061913 (2010)
35. H. Fujita, K. Yamamoto, J. Ohta, Y. Eguchi, K. Yamaguchi, In-plane quantum-dot superlattices of inas on gaassb/gaas (001) for intermediate band solar-cells, in: Proceedings of the 37th IEEE Photovoltaic Specialists Conference (PVSC), 2612-2614 (2011)
36. Tutu, F.K., Wu, J., Lam, P., Tang, M., Miyashita, N., Okada, Y., Wilson, J., Allison, R., Liu, H.: Antimony mediated growth of high-density InAs quantum dots for photovoltaic cells. Appl. Phys. Lett. , **103**, 043901 (2013)
37. Sameshima, K., Sano, T., Yamaguchi, K.: Self-formation of ultrahigh-density (1012 cm-2) inas quantum dots on inassb/gaas (001) and their photoluminescence properties, Appl. Phys. Express **9**, 075501 (2016)
38. Akahane, K., Yamamoto, N., Kawanishi, T.: Fabrication of ultra-high-density inas quantum dots using the strain-compensation technique, Phys. Status Solidi (a) **208**, 425–428 (2011)
39. Sugaya, T., Numakami, O., Oshima, R., Furue, S., Komaki, H., Amano, T., Matsubara, K., Okano, Y., Niki, S.: Ultra-high stacks of InGaAs/GaAs quantum dots for high efficiency solar cells. Energy & Environmental Science **5**, 6233-6237 (2012)
40. Cappelluti, F., Kim, D., van Eerden, M., Cédola, A.P., Aho, T., Bissels, G., Elsehrawy, F., Wu, J., Liu, H., Mulder, P., Bauhuis, G.: Light-trapping enhanced thin-film III-V quantum dot solar cells fabricated by epitaxial lift-off. Sol. Energy Mater. Sol. Cells **181**, 83-92 (2018)

41. Mellor, A., Luque, A., Tobías, I., Martí, A.: The feasibility of high-efficiency inas/gaas quantum dot intermediate band solar cells, Sol. Energy Mater. Sol. Cells **130,** 225–233 (2014)
42. Smith, B.L., Slocum, M.A., Bittner, Z.S., Dai, Y., Nelson, G.T., Hellstroem, S.D., Tatavarti, R., Hubbard, S.M.: Inverted growth evaluation for epitaxial lift off (ELO) quantum dot solar cell and enhanced absorption by back surface texturing. In 2016 IEEE 43rd Photovoltaic Specialists Conference (PVSC), 1276-1281 (2016)
43. Cappelluti, F., Gioannini, M., Ghione, G., Khalili, A.: Numerical study of thin-film quantum-dot solar cells combining selective doping and light-trapping approaches, in 2016 IEEE 43rd Photovoltaic Specialists Conference (PVSC), 1282–1286 (2016)
44. Bennett, M.F., Bittner, Z.S., Forbes, D.V., Tatavarti, S. Rao, Phillip Ahrenkiel, S., Wibowo, A., Pan, N., Chern, K., Hubbard, S.M.: Epitaxial lift-off of quantum dot enhanced gaas single junction solar cells, Appl. Phys. Lett. **103**, 213902 (2013)
45. Sogabe, T., Shoji, Y., Mulder, P., Schermer, J., Tamayo, E., Okada, Y.: Enhancement of current collection in epitaxial lift-off InAs/GaAs quantum dot thin film solar cell and concentrated photovoltaic study. Appl. Phys. Lett. **105**, 113904 (2014)
46. Konagai, M., Sugimoto, M., Takahashi, K.: High efficiency GaAs thin film solar cells by peeled film technology. Journal of crystal growth **45**, 277-280 (1978)
47. Yablonovitch, E., Gmitter, T., Harbison, J.P., Bhat, R.: Extreme selectivity in the lift- off of epitaxial GaAs films. Appl. Phys. Lett. **51**, 2222-2224 (1987)
48. Schermer, J.J., Bauhuis, G.J., Mulder, P., Meulemeesters, W.J., Haverkamp, E., Voncken, M.M.A.J., Larsen, P.K.: High rate epitaxial lift-off of InGaP films from GaAs substrates. Appl. Phys. Lett. **76**, 2131-2133 (2000)
49. Schermer, J.J., Mulder, P., Bauhuis, G.J., Voncken, M.M.A.J., Van Deelen, J., Haverkamp, E., Larsen, P.K.: Epitaxial Lift- Off for large area thin film III/V devices. physica status solidi (a) **202**, 501-508 (2005)
50. Wu, X.S., Coldren, L.A., Merz, J.L.: Selective etching characteristics of HF for AlxGa1-xAs/GaAs. Electron. Lett. **21**, 558-559 (1985)
51. Voncken, M.M.A.J., Schermer, J.J., Bauhuis, G.J., Mulder, P., Larsen, P.K.: Multiple release layer study of the intrinsic lateral etch rate of the epitaxial lift-off process. Appl. Phys. A **79**, 1801-1807 (2004)
52. Smeenk, N.J., Engel, J., Mulder, P., Bauhuis, G.J., Bissels, G.M.M.W., Schermer, J.J., Vlieg, E., Kelly, J.J.: Arsenic formation on GaAs during etching in HF solutions: relevance for the epitaxial lift-off process. ECS J. Solid State Sci. Technol **2**, P58-P65 (2013)
53. Lee, K., Zimmerman, J.D., Xiao, X., Sun, K., Forrest, S.R.: Reuse of GaAs substrates for epitaxial lift-off by employing protection layers. J. Appl. Phys. **111**, 033527 (2012)
54. Horng, R.H., Tseng, M.C., Wu, F.L., Li, C.H., Wu, C.H., Yang, M.D.: Thin film solar cells fabricated using cross-shaped pattern epilayer lift-off technology for substrate recycling applications. IEEE Trans. Electron Devices **59**, 666-672 (2012)
55. Adams, J., Elarde, V., Hains, A., Stender, C., Tuminello, F., Youtsey, C., Wibowo, A., Osowski, M.: Demonstration of multiple substrate reuses for inverted metamorphic solar cells. In 2012 IEEE 38th Photovoltaic Specialists Conference (PVSC), 1-6 (2012)
56. Lee, K., Zimmerman, J.D., Hughes, T.W., Forrest, S.R.: Non- destructive wafer recycling for low- cost thin- film flexible optoelectronics. Advanced Functional Materials **24**, 4284-4291 (2014)
57. Yablonovitch, E., Hwang, D.M., Gmitter, T.J., Florez, L.T., Harbison, J.P.: Van der Waals bonding of GaAs epitaxial liftoff films onto arbitrary substrates. Appl. Phys. Lett. **56**, 2419-2421 (1990)

58. Omnes, F., Guillaume, J.C., Nataf, G., Jager-Waldau, D., Vennegues, P., Gibart, P.: Substrate free GaAs photovoltaic cells on Pd-coated silicon with a 20% AM1. 5 efficiency. IEEE Trans. Electron Devices **43**, 1806-1811 (1996)
59. Lee, X.Y., Goertemiller, M., Boroditsky, M., Ragan, R., Yablonovitch, E.: Thin film GaAs solar cells on glass substrates by epitaxial liftoff. In AIP Conference Proceedings **394**, 719-727 (1997)
60. Schermer, J.J., Mulder, P., Bauhuis, G.J., Larsen, P.K., Oomen, G., Bongers, E.: Thin- film GaAs epitaxial lift- off solar cells for space applications. Progress Photovolt.: Res. Appl. **13**, 587-596 (2005)
61. Schumacher, H., Gmitter, T.J., LeBlanc, H.P., Bhat, R., Yablonovitch, E., Koza, M.A.: High-speed InP/GaInAs photodiode on sapphire substrate. Electronics Letters, **25**, 1653-1654 (1989)
62. Kobayashi, F., Sekiguchi, Y.: GaAs Schottky photodiode fabricated on glass substrate using epitaxial lift-off technique. Japanese journal of applied physics, **31**, L850 (1992)
63. Schnitzer, I., Yablonovitch, E., Caneau, C., Gmitter, T.J., Scherer, A.: 30% external quantum efficiency from surface textured, thin- film light- emitting diodes. Appl. Phys. Lett. **63**, 2174-2176 (1993)
64. Sasaki, Y., Katayama, T., Koishi, T., Shibahara, K., Yokoyama, S., Miyazaki, S., Hirose, M.: High- Speed GaAs Epitaxial Lift- Off and Bonding with High Alignment Accuracy Using a Sapphire Plate. Journal of the electrochemical society **146**, 710-712 (1999)
65. Yablonovitch, E., Kapon, E., Gmitter, T.J., Yun, C.P., Bhat, R.: Double heterostructure GaAs/AlGaAs thin film diode lasers on glass substrates. IEEE Photonics Technology Letters **1**, 41-42 (1989)
66. Pollentier, I., Buydens, L., Van Daele, P., Demeester, P.: Fabrication of a GaAs-AlGaAs GRIN-SCH SQW laser diode on silicon by epitaxial lift-off. IEEE Photonics technology letters **3**, 115-117 (1991)
67. Shah, D.M., Chan, W.K., Caneau, C., Gmitter, T.J., Song, J.I., Hong, B.P., Micelli, P.F., De Rosa, F.: Epitaxial lift-off GaAs HEMT's. IEEE Trans. Electron Devices **42**, 1877-1881 (1995)
68. Morf, T., Biber, C., Bachtold, W.: Effects of epitaxial lift-off on the DC, RF, and thermal properties of MESFET's on various host materials. IEEE Trans. Electron Devices **45**, 1407-1413 (1998)
69. Georgiou, G., Tyagi, H.K., Mulder, P., Bauhuis, G.J., Schermer, J.J., Rivas, J.G.: Photo-generated THz antennas. Scientific reports **4**, 3584 (2014)
70. Voncken, M.M.A.J., Schermer, J.J., Bauhuis, G.J., Van Niftrik, A.T.J., Larsen, P.K.: Strain-accelerated HF etching of AlAs for epitaxial lift-off. Journal of Physics: Condensed Matter **16**, 3585 (2004)
71. Van Niftrik, A.T., Schermer, J.J., Bauhuis, G.J., van Deelen, J., Mulder, P., Larsen, P.K.: The Influence of In x Ga1–x As and GaAs1–y P y Layers Surrounding the AlAs Release Layer in the Epitaxial Lift-Off Process. Crystal Growth and Design **7**, 2472-2480 (2007)
72. Bauhuis, G.J., Mulder, P., Schermer, J.J.: Thin-film iii–v solar cells using epitaxial lift-off. In High-Efficiency Solar Cells. Springer, Cham., 623-643 (2014)
73. Voncken, M.M.A.J., Schermer, J.J., Van Niftrik, A.T.J., Bauhuis, G.J., Mulder, P., Larsen, P.K., Peters, T.P.J., De Bruin, B., Klaassen, A., Kelly, J.J.: Etching AlAs with HF for epitaxial lift-off applications. Journal of the Electrochemical Society **151**, G347-G352 (2004)
74. Van Niftrik, A.T.J., Schermer, J.J., Bauhuis, G.J., Mulder, P., Larsen, P.K., Kelly, J.J.: A diffusion and reaction related model of the epitaxial lift-off process. Journal of the Electrochemical Society **154**, D629-D635 (2007)

75. Voncken, M.M.A.J., Schermer, J.J., Maduro, G., Bauhuis, G.J., Mulder, P., Larsen, P.K.: Influence of radius of curvature on the lateral etch rate of the weight induced epitaxial lift-off process. Materials Science and Engineering: B **95**, 242-248 (2002)
76. Van Niftrik, A.T.J., Schermer, J.J., Bauhuis, G.J., Mulder, P., Larsen, P.K., Van Setten, M.J., Attema, J.J., Tan, N.C.G., Kelly, J.J.: HF species and dissolved oxygen on the epitaxial lift-off process of GaAs using AlAsP release layers. Journal of The Electrochemical Society **155**, D35-D39 (2008)
77. Tatavarti, R., Hillier, G., Martin, G., Wibowo, A., Navaratnarajah, R., Tuminello, F., Hertkorn, D., Disabb, M., Youtsey, C., McCallum, D., Pan, N.: Lightweight, low cost InGaP/GaAs dual-junction solar cells on 100 mm epitaxial liftoff (ELO) wafers. In 2009 34th IEEE Photovoltaic Specialists Conference (PVSC), 2065-2067 (2009)
78. Youtsey, C., Adams, J., Chan, R., Elarde, V., Hillier, G., Osowski, M., McCallum, D., Miyamoto, H., Pan, N., Stender, C., Tatavarti, R.: Epitaxial lift-off of large-area GaAs thin-film multi-junction solar cells. In Proc. of the CS MANTECH Conference (2012)
79. Van Leest, R.H., Mulder, P., Gruginskie, N., van Laar, S.C., Bauhuis, G.J., Cheun, H., Lee, H., Yoon, W., van der Heijden, R., Bongers, E., Vlieg, E.: Temperature-induced degradation of thin-film III–V solar cells for space applications. IEEE J. Photovolt. **7**, 702-708 (2017)
80. Farah, J.: Dry-epitaxial lift-off, integration, interconnect and encapsulation of foldable/rollable high efficiency solar cell modules. In 2012 38th IEEE Photovoltaic Specialists Conference, 2868-2873 (2012)
81. Trautz, K.M., Jenkins, P.P., Walters, R.J., Scheiman, D., Hoheisel, R., Tatavarti, R., Chan, R., Miyamoto, H., Adams, J.G., Elarde, V.C., Grimsley, J.: Mobile solar power. IEEE J. Photovolt. **3**, 535-541 (2012)
82. Essig, S., Steiner, M.A., Allebé, C., Geisz, J.F., Paviet-Salomon, B., Ward, S., Descoeudres, A., LaSalvia, V., Barraud, L., Badel, N., Faes, A.: Realization of GaInP/Si dual-junction solar cells with 29.8% 1-sun efficiency. IEEE J. Photovolt. **6**, 1012-1019 (2016)
83. Hannappel, T., Sagol, B.E., Seidel, U., Szabo, N., Schwarzburg, K., Bauhuis, G.J., Mulder, P.: Measurement of an InGaAsP/InGaAs tandem solar cell under GaAs. In 2008 33rd IEEE Photovoltaic Specialists Conference, 1-3 (2008)
84. Essig, S., Allebé, C., Remo, T., Geisz, J.F., Steiner, M.A., Horowitz, K., Barraud, L., Ward, J.S., Schnabel, M., Descoeudres, A., Young, D.L.: Raising the one-sun conversion efficiency of III–V/Si solar cells to 32.8% for two junctions and 35.9% for three junctions. Nature Energy **2**, 17144 (2017)
85. Schermer, J.J., Bauhuis, G.J., Mulder, P., Haverkamp, E.J., Van Deelen, J., Van Niftrik, A.T.J., Larsen, P.K.: Photon confinement in high-efficiency, thin-film III–V solar cells obtained by epitaxial lift-off. Thin Solid Films **511**, 645-653 (2006)
86. Bauhuis, G.J., Schermer, J.J., Mulder, P., Voncken, M.M.A.J., Larsen, P.K.: Thin film GaAs solar cells with increased quantum efficiency due to light reflection. Sol. Energy Mater. Sol. Cells **83**, 81-90 (2004)
87. Tatavarti, R., Wibowo, A., Elarde, V., Tuminello, F., Pastor, R., Giannopoulos, T., Osowski, M., Chan, R., Youtsey, C., Hillier, G., Pan, N.: Large-area, epitaxial lift-off, inverted metamorphic solar cells. In 2011 37th IEEE Photovoltaic Specialists Conference, 1941-1944 (2011)
88. Asbeck, P.: Self- absorption effects on the radiative lifetime in GaAs- GaAlAs double heterostructures. J. Appl. Phys. **48**, 820-822 (1977)
89. Ahrenkiel, R.K., Dunlavy, D.J., Keyes, B., Vernon, S.M., Dixon, T.M., Tobin, S.P., Miller, K.L., Hayes, R.E.: Ultralong minority- carrier lifetime epitaxial GaAs by photon recycling. Appl. Phys. Lett. **55**, 1088-1090 (1989)

90. Parrott, J.E.: Radiative recombination and photon recycling in photovoltaic solar cells. Sol. Energy Mater. Sol. Cells **30**, 221-231 (1993)
91. Lush, G.B.: B-coefficient in n-type GaAs. Sol. Energy Mater. Sol. Cells **93**, 1225-1229 (2009)
92. Bauhuis, G.J., Mulder, P., Haverkamp, E.J., Huijben, J. C. C. M., Schermer, J.J.: 26.1% thin-film GaAs solar cell using epitaxial lift-off. Sol. Energy Mater. Sol. Cells **93**, 1488-1491 (2009)
93. Geisz, J. F., Steiner, M. A., Garcia, I., Kurtz, S. R., Friedman, D. J.: Enhanced external radiative efficiency for 20.8% efficient single-junction GaInP solar cells. Appl. Phys. Lett. **103**, 041118 (2013)
94. Steiner, M. A., Geisz, J. F., Garcia, I., Friedman, D. J., Duda, A., Kurtz, S. R.: Optical enhancement of the open-circuit voltage in high quality GaAs solar cells. J. Appl. Phys. **113**, 123109 (2013)
95. Lumb, M. P., Steiner, M. A., Geisz, J. F., Walters, R. J.: Incorporating photon recycling into the analytical drift-diffusion model of high efficiency solar cells. J. Appl. Phys. **116**, 194504 (2014)
96. Bauhuis, G., Mulder, P., Hu, Y.Y., Schermer, J.: Deep junction III–V solar cells with enhanced performance. physica status solidi (a) **213**, 2216-2222 (2016)
97. Bailey, C.G., Forbes, D.V., Raffaelle, R.P., Hubbard, S.M.: Near 1 V open circuit voltage InAs/GaAs quantum dot solar cells. Appl. Phys. Lett. **98**, 163105 (2011)
98. Sablon, K.A., Little, J.W., Olver, K.A., Wang, Z.M., Dorogan, V.G., Mazur, Y.I., Salamo, G.J., Towner, F.J.: Effects of AlGaAs energy barriers on InAs/GaAs quantum dot solar cells. J. Appl. Phys. **108**, 74305 (2010)
99. Lam, P., Wu, J., Tang, M., Jiang, Q., Hatch, S., Beanland, R., Wilson, J., Allison, R., Liu, H.: Submonolayer InGaAs/GaAs quantum dot solar cells. Sol. Energy Mater. Sol. Cells **126**, 83-87 (2014)
100. Tukiainen, A., Lyytikäinen, J., Aho, T., Halonen, E., Raappana, M., Cappelluti, F., Guina, M.: Comparison of 'shallow'and 'deep'junction architectures for MBE-grown InAs/GaAs quantum dot solar cells. In 2018 IEEE 7th World Conference on Photovoltaic Energy Conversion (WCPEC)(A Joint Conference of 45th IEEE PVSC, 28th PVSEC & 34th EU PVSEC), 2950-2952 (2018)
101. Levy, M.Y., Honsberg, C.: Solar cell with an intermediate band of finite width. Phys. Rev. B, **78**, 165122 (2008)
102. Cuadra, L., Martí, A., Luque, A.: Influence of the overlap between the absorption coefficients on the efficiency of the intermediate band solar cell. IEEE Trans. Electron Devices **51**, 1002-1007 (2004)
103. Strandberg, R., Reenaas, T.: Optimal filling of the intermediate band in idealized intermediate-band solar cells. IEEE Trans. Electron Devices **58**, 2559-2565 (2011)
104. Yoshida, K., Okada, Y., Sano, N.: Self-consistent simulation of intermediate band solar cells: Effect of occupation rates on device characteristics. Appl. Phys. Lett. **97**, 133503 (2010)
105. Lin, A.S., Phillips, J.D.: Drift-diffusion modeling for impurity photovoltaic devices. IEEE Trans. Electron Devices **56**, 3168-3174 (2009)
106. Strandberg, R., Reenaas, T.W.: Drift- diffusion model for intermediate band solar cells including photofilling effects. Progress Photovolt.: Res. Appl. **19**, 21-32 (2011)
107. Zhu, L., Akiyama, H., Kanemitsu, Y.: Intrinsic and extrinsic drops in open-circuit voltage and conversion efficiency in solar cells with quantum dots embedded in host materials. Scientific reports **8**, 11704 (2018)
108. Aeberhard, U.: Simulation of nanostructure-based high-efficiency solar cells: challenges, existing approaches, and future directions. IEEE J. Sel. Top. Quantum Electron. **19**, 1-11 (2013)

109. Walker, A.W., Thériault, O., Hinzer, K.: The dependence of multijunction solar cell performance on the number of quantum dot layers. IEEE J. Quantum Electron. **50**, 198-203 (2014)
110. Gioannini, M., Cedola, A.P., Di Santo, N., Bertazzi, F., Cappelluti, F.: Simulation of quantum dot solar cells including carrier intersubband dynamics and transport. IEEE J. of Photovolt. **3**, 1271-1278 (2013)
111. Cappelluti, F., Gioannini, M., Khalili, A.: Impact of doping on inas/gaas quantum-dot solar cells: a numerical study on photovoltaic and photoluminescence behavior, Sol. Energy Mater. Sol. Cells **157**, 209-220 (2016).
112. Cédola, A.P., Kim, D., Tibaldi, A., Tang, M., Khalili, A., Wu, J., Liu, H., Cappelluti, F.: Physics-based modeling and experimental study of si-doped inas/gaas quantum dot solar cells. Int. J. Photoenergy, (2018)
113. Khalili, A., Tibaldi, A., Elsehrawy, F., Cappelluti, F.: Multiscale device simulation of quantum dot solar cells. In Physics, Simulation, and Photonic Engineering of Photovoltaic Devices VIII 10913, 109131N. International Society for Optics and Photonics, (2019)
114. Jolley, G., Fu, L., Lu, H. F., Tan, H. H., Jagadish, C.: The role of intersubband optical transitions on the electrical properties of ingaas/gaas quantum dot solar cells, Progress Photovolt.: Res. Appl. **21**, 736-746 (2013).
115. Khalili, A., Cappelluti, F.: Modeling of type-ii quantum dot intermediate band solar cells accounting for thermal and optical intersubband transitions, in 2018 International Conference on Numerical Simulation of Optoelectronic Devices (NUSOD), 139-140 (2018).
116. Hwang, J., Martin, A. J., Millunchick, J. M., Phillips, J. D.: Thermal emission in type-ii gasb/gaas quantum dots and prospects for intermediate band solar energy conversion, J. Appl. Phys. **111**, 074514 (2012)
117. Williamson, A.J., Wang, L.W., Zunger, A.: Theoretical interpretation of the experimental electronic structure of lens-shaped self-assembled InAs/GaAs quantum dots. Phys. Rev. B **62**, 12963 (2000)
118. King, R.R., Bhusari, D., Boca, A., Larrabee, D., Liu, X.Q., Hong, W., Fetzer, C.M., Law, D.C., Karam, N.H.: Band gap- voltage offset and energy production in next- generation multijunction solar cells. Progress Photovolt.: Res. Appl. **19**, 797-812 (2011)
119. Ekins-Daukes, N., Pusch, A.: The Use and Abuse of W_{oc} as a Figure of Merit, Proceedings of PVSEC 2018, (2018)
120. Nuntawong, N., Tatebayashi, J., Wong, P.S., Huffaker, D.L.: Localized strain reduction in strain-compensated In As⁄ Ga As stacked quantum dot structures. Appl. Phys. Lett. **90**, 163121 (2007)
121. Bowen, D.K., Tanner, B.K.: High resolution X-ray diffractometry and topography. CRC press (2005)
122. Fewster, P. F.: X-ray diffraction from multiple quantum well structures, Philips Journal of Research **41**, 268–289 (1986).
123. Gee, J.M.: The effect of parasitic absorption losses on light trapping in thin silicon solar cells, in: Proceedings of the 2016 IEEE Conference Record of the Twentieth IEEE Photovoltaic Specialists Conference **1**, 549–554 (1988)
124. Green, M.A.: Lambertian light trapping in textured solar cells and light-emitting diodes: analytical solutions, Progress. Photovolt.: Res. Appl. **10**, 235–241 (2002)
125. Weber, M.J.: Handbook of Optical Materials. CRC press, Boca Raton, Florida (2002)
126. Tsai, C., Liu, G., Fan, G., Lee, Y.: Substrate-free large gap InGaN solar cells with bottom reflector. Solid-State Electron. **54**, 541-544 (2010)

127. Vandamme, N., Hung-Ling, C., Gaucher, A., Behaghel, B., Lemaitre, A., Cattoni, A., Dupuis, C., Bardou, N., Guillemoles, J., Collin, S.: Ultrathin GaAs solar cells with a silver back mirror. IEEE J. Photovoltaics **5**, 565-570 (2015)
128. Baca, A.G., Ashby, C.I.: Fabrication of GaAs Devices. IET, London (2005)
129. Van Leest, R.H., Bauhuis, G.J., Mulder, P., van der Heijden, R., Bongers, E., Vlieg, E., Schermer, J.J.: Effects of copper diffusion in gallium arsenide solar cells for space applications. Sol. Energy Mater. Sol. Cells **140**, 45-53 (2015)
130. Van Leest, R.H., de Kleijne, K., Bauhuis, G.J., Mulder, P., Cheun, H., Lee, H., Yoon, W., van der Heijden, R., Bongers, E., Vlieg, E., Schermer, J.J.: Degradation mechanism (s) of GaAs solar cells with Cu contacts. Phys. Chem. Chem. Phys. **18**, 10232-10240 (2016)
131. Aho, T., Aho, A., Tukiainen, A., Polojärvi, V., Salminen, T., Raappana, M., Guina, M.: Enhancement of photocurrent in GaInNAs solar cells using Ag/Cu double-layer back reflector. Appl. Phys. Lett. **109**, 251104 (2016)
132. ASTM Standard, "Standard tables for reference solar spectral irradiances: Direct normal and hemispherical on 37◦ tilted surface," ASTM International, Tech. Rep. **12**, (2008)
133. Stareev, G., Künzel, H., Dortmann, G.: A controllable mechanism of forming extremely low- resistance nonalloyed ohmic contacts to group III- V compound semiconductors. J. Appl. Phys. **74**, 7344-7356 (1993)
134. Akdogan, I.G., Parker, M.A.: Au-Cu Ohmic Contacts for p+ GaAs. Electrochem. Solid-State Lett. **8**, G106-G108 (2005)
135. Inoue, T., Watanabe, K., Toprasertpong, K., Fujii, H., Sugiyama, M., Nakano, Y.: Enhanced light trapping in multiple quantum wells by thin-film structure and backside grooves with dielectric interface. IEEE J. Photovolt. **5,** 697–703 (2015)
136. Mokkapati, S., Catchpole, K. R.: Nanophotonic light trapping in solar cells. J. Appl. Phys. **112**, 101101 (2012)
137. Palanchoke, U., Jovanov, V., Kurz, H., Obermeyer, P., Stiebig, H., Knipp, D.: Plasmonic effects in amorphous silicon thin film solar cells with metal back contacts. Opt. Express **20**, 6340-6347 (2012)
138. Tommila, J., Polojärvi, V., Aho, A., Tukiainen, A., Viheriälä, J., Salmi, J., Schramm, A., Kontio, J., Turtiainen, A., Niemi, T.: Nanostructured broadband antireflection coatings on AlInP fabricated by nanoimprint lithography. Solar Energy Mater. Solar Cells **94**, 1845-1848 (2010)
139. Musu, A., Cappelluti, F., Aho, T., Polojärvi, V., Niemi, T., Guina, M.: Nanostructures for light management in thin-film GaAs quantum dot solar cells. OSA Light, Energy and the Environment Congress, JW4A-45 (2016)
140. RSoft Design Group: DiffractMOD. <https://www.synopsys.com/optical-solutions/rsoft/passive-device-diffractMOD.html>.
141. Elsehrawy, F., Cappelluti, F., Aho, T., Niemi, T., Polojärvi, V., Guina, M.: Back grating optimization for light trapping in thin-film quantum dot solar cells. 19th Italian National Conference on Photonic Technologies, 34 (2017)
142. Elsehrawy, F., Aho, T., Niemi, T., Guina, M., & Cappelluti, F. (2018, November). Improved Light Trapping in Quantum Dot Solar Cells Using Double-sided Nanostructuring. In Optics and Photonics for Energy and the Environment (pp. JM4A-5). Optical Society of America.
143. Aho, T., Guina, M., Elsehrawy, F., Cappelluti, F., Raappana, M., Tukiainen, A., Alam, A.K., Vartiainen, I., Kuittinen, M., Niemi, T.: Comparison of metal/polymer back reflectors with half-sphere, blazed, and pyramid gratings for light trapping in III-V solar cells. Opt. Express **26**, A331-A340 (2018)

144. Ganapati, V., Steiner, M.A., Yablonovitch, E.: The voltage boost enabled by luminescence extraction in solar cells. IEEE J. Photovolt. **6**, 801-809 (2016)
145. Gruginskie, N., van Laar, S.C.W., Bauhuis, G., Mulder, P., van Eerden, M., Vlieg, E., Schermer, J.J.: Increased performance of thin-film GaAs solar cells by rear contact/mirror patterning. Thin Solid Films **660**, 10-18 (2018)
146. M. van Eerden, G. Bauhuis, P. Mulder, N. Gruginskie, M. Passoni, L.C. Andreani, E. Vlieg, Schermer, J.J.: A facile light trapping approach for ultra-thin GaAs solar cells using wet chemical etching. Submitted to Progress in Photovoltaics (2019)
147. Stender, C.L., Adams, J., Elarde, V., Major, T., Miyamoto, H., Osowski, M., Pan, N., Tatavarti, R., Tuminello, F., Wibowo, A., Youtsey, C.: Flexible and lightweight epitaxial lift-off GaAs multi-junction solar cells for portable power and UAV applications. In 2015 IEEE 42nd Photovoltaic Specialist Conference (PVSC), 1-4 (2015)
148. Scheiman, D., Hoheisel, R., Edwards, D.J., Paulsen, A., Lorentzen, J., Jenkins, P., Caruthers, S., Carter, S., Walters, R.: A path toward enhanced endurance of a UAV using IMM solar cells. In 2016 IEEE 43rd Photovoltaic Specialists Conference (PVSC), 1095-1100 (2016)
149. PV Magazine: Audi, Hanergy unit to jointly develop PV for vehicles. <http://pv-magazine.com/2017/08/23/audi-hanergy-unit-to-jointly-develop-pv-for-vehicles>
150. US Department of Energy, Office of Energy Efficiency and Renewable Energy: High-Efficiency, Low-Cost, One-Sun, III-V Photovoltaics. <http://energy.gov/eere/solar/project-profile-high-efficiency-low-cost-one-sun-iii-v-photovoltaics>